

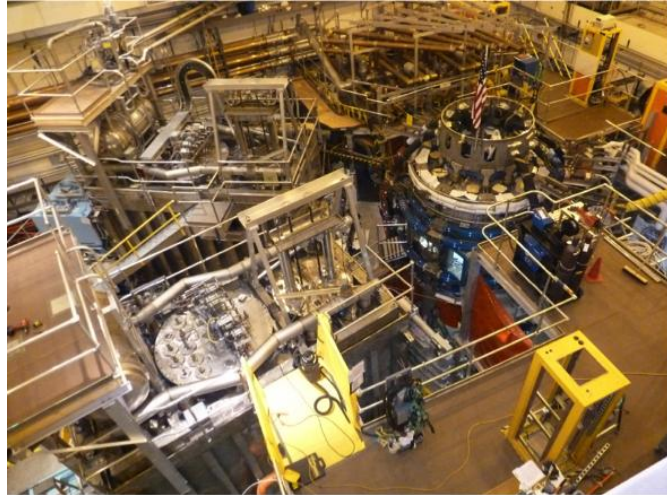
Table of Contents for Chapter 10

10.1. Introduction.....	3
10.2. Overview of Facility and Diagnostics.....	4
10.3. NSTX Upgrade Project Status and Plan	6
10.3.1. New Center Stack Upgrade.....	9
10.3.1.1. New Center Stack Fabrication	9
10.3.1.2. NSTX-U Device Structural Enhancements	12
10.3.2. Second Neutral Beam Injection System Upgrade.....	14
10.3.3. NSTX-U Facility Subsystems.....	17
10.3.3.1. TF and OH Power Systems for NSTX Upgrade	17
10.3.3.2. Rectifier Control System Upgrades	18
10.3.3.3. Poloidal Field Coil Power Supply Upgrades	19
10.3.3.4. Migrate Plasma Control System to Modern Processors	20
10.4. RF Heating and Current Drive Systems.....	20
10.4.1. HHFW Upgrades	21
10.4.2. Electron Cyclotron / Electron Bernstein Wave Heating System	22
10.5 Facility Science Tools.....	23
10.5.1. Macro-stability Tools.....	23
10.5.1.1. 2nd Switching Power Amplifier (SPA)	24
10.5.1.2. Non-axisymmetric Control Coils.....	24
10.5.1.3. Disruption Mitigation Systems	25
10.5.2. Boundary Physics Tools	27
10.5.2.1. Divertor Cryo-pump.....	28
10.5.2.2. EHO antenna.....	29
10.5.2.3. Fueling Tools	29
10.5.2.4. Lithium Granule Injector for ELM Control.....	31
10.5.2.5. Lithium Evaporator and Upgraded Lithium Coating Systems	32
10.5.2.6. High-Z Metallic Divertor.....	33
10.5.2.7. High-Z Outer and Inner Wall PFCs.....	33
10.5.2.8. Flowing Liquid Lithium Divertor/Module.....	34
10.5.2.9. Laboratories for Material Characterization and Surface Chemistry	35
10.5.3. Start-up and Ramp-up.....	36

NSTX Upgrade Research Plan for 2014-2018

10.5.3.1. CHI upgrades	36
10.5.3.2. Plasma Gun Start-Up	37
10.6 NSTX-U Diagnostic System Status and Plans	38
10.6.1. Profile Diagnostics.....	39
10.6.1.1. Multi-Pulse Thompson Scattering System.....	39
10.6.1.2. Charge-Exchange Recombination Spectroscopy.....	40
10.6.1.3. Soft X-ray Diagnostics.....	42
10.6.1.4. Motional Stark Effect – Collisional Induced Fluorescence	43
10.6.1.5. Motional Stark Effect – Laser Induced Fluorescence.....	44
10.6.2. Turbulence Diagnostics	45
10.6.2.1. High-k Scattering System	46
10.6.2.2. Beam Emission Spectroscopy.....	47
10.6.2.3. Microwave Polarimeter Magnetic Fluctuation Diagnostic	48
10.6.2.4. Gas Puff Imaging Diagnostic.....	48
10.6.3. MHD / ASC Diagnostics	48
10.6.3.1. Magnetics For Equilibrium Reconstruction, Boundary Control, and RWM Suppression.....	49
10.6.3.2. Real-Time Velocity Diagnostic	49
10.6.3.3. Real time MSE (rtMSE).....	50
10.6.3.4. Real-Time Multi-Pulse Thomson Scattering (rtMPTS).....	50
10.6.3.5. Real-Time Density Interferometry.....	51
10.6.3.6. Diagnostics for disruption mitigation experiments.....	51
10.6.4. Boundary Physics Diagnostics.....	53
10.6.4.1. Material Analysis Particle Probe (MAPP).....	53
10.6.4.2. Divertor Spectrometers and Two-Color Fast Infrared Camera.....	54
10.6.4.3. Dust Detector and Quartz Crystal Microbalances	56
10.6.4.4. Divertor Thomson Scattering System.....	57
10.6.5. Energetic Particle Diagnostics	58
10.6.5.1. Energetic Particle Distribution Diagnostics.....	58
10.6.5.2 Energetic-Particle-Induced Mode Diagnostics	60
10.6.5.3. Alfvén Eigenmode Antenna for AE Stability Measurements.....	62
10.7. NSTX-U Plasma Operation Start-Up Plan	63
References.....	65

Chapter 10



NSTX-U

Facility Status and Proposed Upgrades

10.1. Introduction

The National Spherical Torus Experiment Upgrade (NSTX-U) is the world's leading spherical tokamak, combining an exceptionally wide plasma parameter space, a high degree of facility flexibility, and state-of-the-art diagnostic systems. Presently, the NSTX-U is undergoing a major upgrade construction with a new and more powerful center-stack and a tangentially injecting 2nd Neutral Beam Injection (NBI) system. The upgraded NSTX or NSTX-U will double the toroidal field from ~ 0.5 T to 1 T, the plasma current from ~ 1 MA to 2 MA, the NBI heating and current drive power from ~ 7 MW to 14 MW, and greatly increase the peak field plasma pulse length from 1 sec to 7 sec. The present upgrade construction is scheduled to be completed in the summer of 2014. These upgrades are aimed at achieving fully non-inductively sustained, long-pulse high-performance operation and exploring an expanded plasma parameter space in terms of higher plasma temperature and lower collisionality. The new physics regimes made accessible by these upgrades will significantly reduce the gap, and thus the uncertainty in extrapolating, from the present NSTX to projected next-step ST experiments such as the Fusion Nuclear Science Facility. From the beginning of the NSTX-U operation, it will have the capability of 6 MW High-Harmonic Fast Waves (HHFW) heating and current drive system and the coaxial helicity injection (CHI) with a project start-up current of 400 kA. In addition to advanced plasma shaping capabilities, NSTX is equipped with a set of six non-axisymmetric control coils which can be independently controlled by the Switching Power Amplifier (SPA) sources to enhance plasma stability and is also exploring and developing the use of lithium as a plasma facing material. Additional major facility hardware and diagnostic systems are proposed for the Five Year Plan to

fully take advantage of the NSTX-U facility capabilities as shown in Fig. 10.1. Attracted by its unique capabilities, NSTX-U plans to host a large number of national and international researchers (over 250 annually) with over 55 institutions participating in the research program. Nationally, the team members are from 30 universities, national laboratories, and industries. The collaborating institutions will be providing about half of the NSTX-U diagnostic systems.

10.2. Overview of Facility and Diagnostics

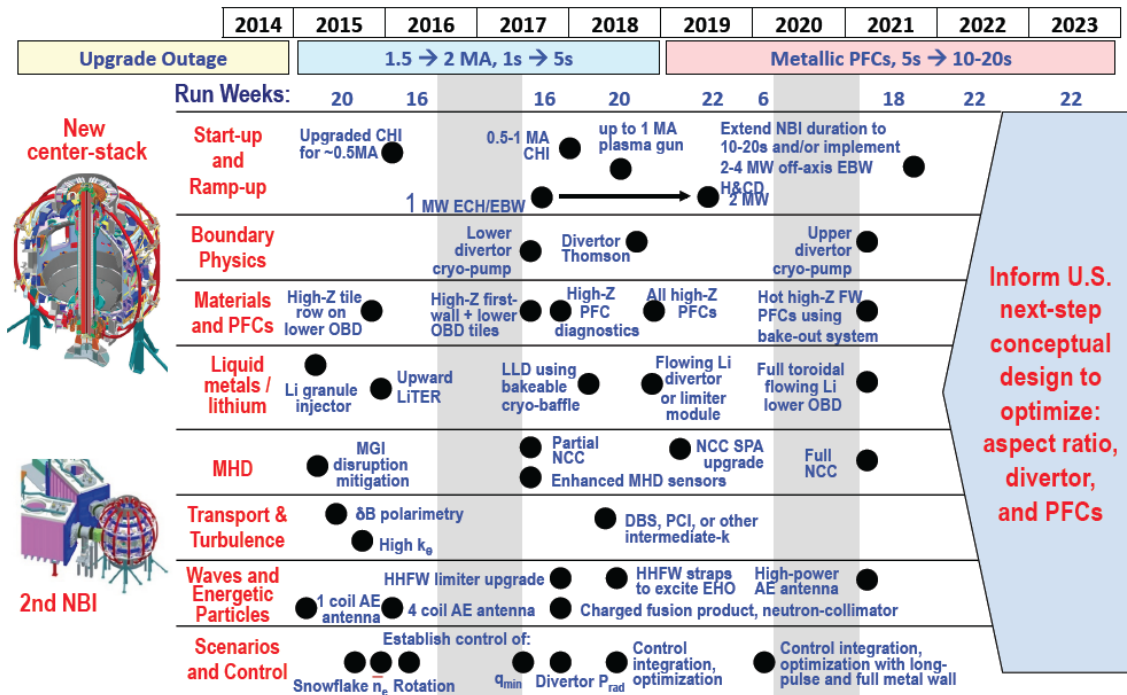


Fig. 10.1 Long-range facility upgrade vision for NSTX-U supporting ITER and FNSF with 5 YP incremental funding.

There are a number of important facility related enhancements which are needed to take full advantage of the NSTX-U device capabilities as shown in Fig. 10.1. In preparation for the NSTX-U operations and for the 2014-18 Five Year Plan, the NSTX-U facility enhancement brainstorming meeting was held on Feb. 7 and 8, 2012. Many innovative ideas were proposed to support and enhance the NSTX-U 5 Year Research Plan. In the start-up area, the CHI capability will be readied with a base capability of 0.3 – 0.5 MA level. Further CHI upgrade for higher start-up current level for 0.5 – 1.0 MA will be implemented after the initial assessment of the performance of the base CHI system on NSTX-U. The plasma gun start-up being developed by the PEGASUS group will be implemented on NSTX-U at 0.2 – 0.4 MA level start-up capability when it is technically ready.

NSTX Upgrade Research Plan for 2014-2018

Further upgrades toward 1 MA start-up current for the plasma gun will be assessed after the initial gun performance on NSTX-U. A MW-class 28 GHz ECH/EBW system will be implemented at high priority to assist the start-up and ramp-up research. With favorable results, the system will be upgraded to 2 MW level to provide off-axis current drive for current profile control. For boundary physics, the divertor cryo-pump will be installed for increased particle pumping at the lower divertor after the initial operation. The divertor Thomson scattering system will be implemented as resources become available. For Materials and PFCs, the moly tiles will first be implemented in the lower divertor. After the initial assessment, the moly tile installation for both upper and lower divertor will be implemented and coverage of the first-wall with high-Z PFCs will be increased. For lithium capability, the baseline is the dual upper (lower aiming) evaporators as in NSTX. A design will be developed for an upper aiming evaporator to cover the upper divertor region. The lithium granular injector for ELM pacing which was successfully demonstrated on EAST will be available for NSTX-U. Various concepts are being considered for liquid lithium divertor system. A flowing liquid lithium loop R&D facility supported by LDRD (laboratory internal funding) is being built at PPPL. If successful, the design will be adapted for NSTX-U. The HT-7 tokamak is also testing liquid lithium PFCs. For MHD research, the massive gas injector disruption mitigation system will be implemented while the resonant field amplification (RFA) / resistive wall mode (RWM) sensors will be enhanced. For a longer term upgrade, the non-axisymmetric control coil (NCC) system is being considered and a conceptual design of NCC is being developed. For Transport and Turbulence research, an upgraded high-k scattering system with significant κ_θ component will be implemented along with a 48 channel BES for low-k turbulence measurements. A microwave polarimeter will be installed for magnetic fluctuation measurements. For high harmonic fast wave (HHFW) research, antenna enhancements are being performed to enable the HHWF feed-thru conductor to

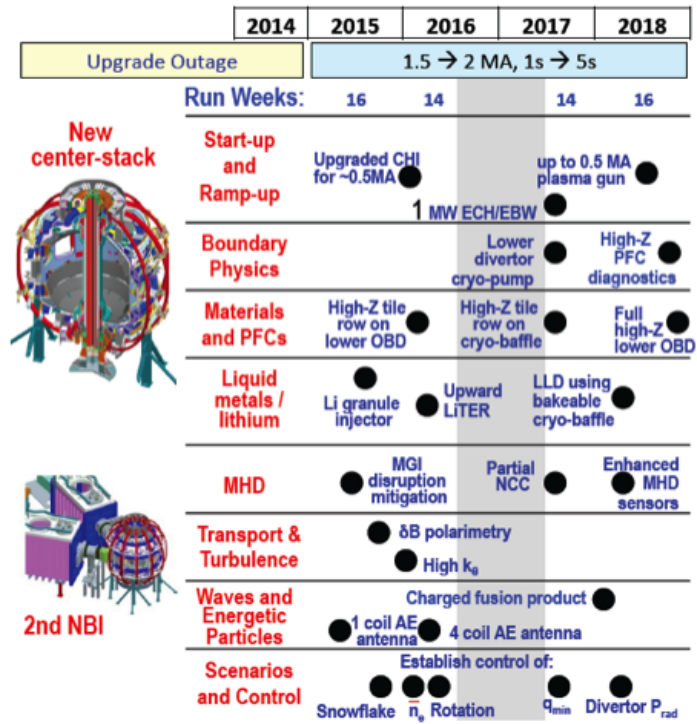


Fig. 10.2 Long-range facility upgrade vision for NSTX-U supporting ITER and FNSF with 5 YP base funding.

Further upgrades toward 1 MA start-up current for the plasma gun will be assessed after the initial gun performance on NSTX-U. A MW-class 28 GHz ECH/EBW system will be implemented at high priority to assist the start-up and ramp-up research. With favorable results, the system will be upgraded to 2 MW level to provide off-axis current drive for current profile control. For boundary physics, the divertor cryo-pump will be installed for increased particle pumping at the lower divertor after the initial operation. The divertor Thomson scattering system will be implemented as resources become available. For Materials and PFCs, the moly tiles will first be implemented in the lower divertor. After the initial assessment, the moly tile installation for both upper and lower divertor will be implemented and coverage of the first-wall with high-Z PFCs will be increased. For lithium capability, the baseline is the dual upper (lower aiming) evaporators as in NSTX. A design will be developed for an upper aiming evaporator to cover the upper divertor region. The lithium granular injector for ELM pacing which was successfully demonstrated on EAST will be available for NSTX-U. Various concepts are being considered for liquid lithium divertor system. A flowing liquid lithium loop R&D facility supported by LDRD (laboratory internal funding) is being built at PPPL. If successful, the design will be adapted for NSTX-U. The HT-7 tokamak is also testing liquid lithium PFCs. For MHD research, the massive gas injector disruption mitigation system will be implemented while the resonant field amplification (RFA) / resistive wall mode (RWM) sensors will be enhanced. For a longer term upgrade, the non-axisymmetric control coil (NCC) system is being considered and a conceptual design of NCC is being developed. For Transport and Turbulence research, an upgraded high-k scattering system with significant κ_θ component will be implemented along with a 48 channel BES for low-k turbulence measurements. A microwave polarimeter will be installed for magnetic fluctuation measurements. For high harmonic fast wave (HHFW) research, antenna enhancements are being performed to enable the HHWF feed-thru conductor to

handle the higher disruption loads ($\sim x 4$) in NSTX-U. A HHFW poloidal limiter upgrade to handle higher power and longer pulse NBI power is also considered for NSTX-U. Antennas for EHO and *AE excitations will also be considered after initial assessments. For Advanced Scenario and Control area, the real time plasma control system and real time diagnostic systems will be implemented for snowflake, density, rotation, and q-profile control. With the base budget without the increment, the implemental plan will be delayed as shown in Fig. 10.2. Note that several long-range facility upgrades will be delayed beyond FY 2018 in this budget scenario.

10.3. NSTX Upgrade Project Status and Plan

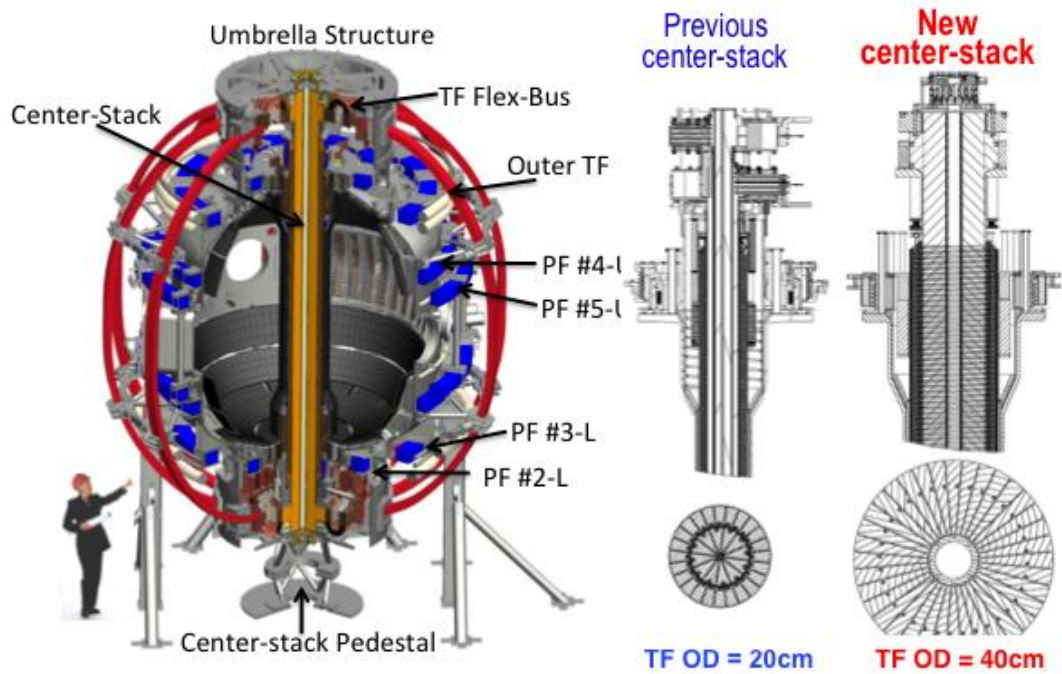
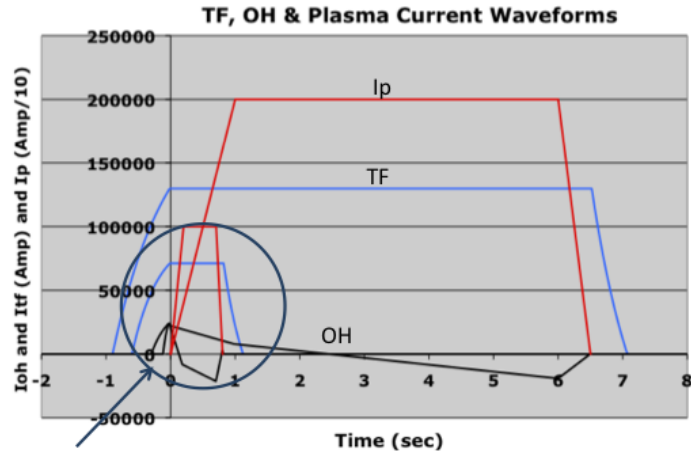


Fig. 10.3 A schematic of the NSTX-U device.

Fig. 10.4. Comparison of the new center-stack for NSTX-U and the previous one for NSTX.

The NSTX facility is presently undergoing a major upgrade with construction of a new and more powerful center-stack and a tangentially injection 2nd Neutral Beam Injection (NBI) system. The upgraded NSTX or NSTX-U will double the toroidal field from ~ 0.5 T to 1 T, the plasma current from ~ 1 MA to 2 MA, the NBI heating and current drive power from ~ 7 MW to 14 MW, and greatly increase the peak field plasma pulse length from 1 sec to 7 sec [1].



Present NSTX

Fig. 10.5. NSTX and NSTX-U TF, OH, & Plasma Current Waveforms.

Schematics of the NSTX-U device and the new upgrade center-stack cross-section along with the previous one on NSTX are shown in Figs. 10.3 and 10.4. The larger (nearly $\times 4$) TF conductor size enables the doubling of the toroidal field and much more extended pulse length. The larger OH solenoid radius ($\sim \times 2$) enables $\sim \times 3$ OH flux needed to support higher longer pulse plasma current as shown in Fig. 10.5. The injection geometry of the second NBI along with the existing NBI system on NSTX is shown in Fig. 10.6. The tangential injection angles of the 2nd NBI enables much higher ($\sim 2\times$) plasma current drive efficiency and current profile control needed for the fully non-inductive advanced plasma operation. In Fig. 10.7, the general arrangement of the NSTX-U Test Cell is shown with the 2nd NBI.

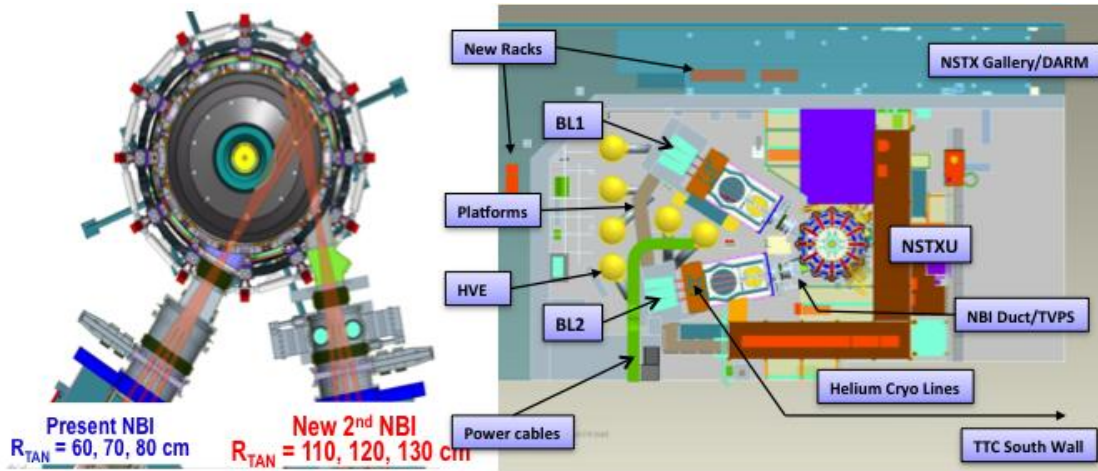


Fig. 10.6. The injection geometry of the new tangential 2nd NBI compared to the present more perpendicular NBI.

Fig. 10.7. NSTX-U Test Cell general arrangement schematic drawing with key 2nd NBI system components.

NSTX Upgrade Research Plan for 2014-2018

On February 23, 2009, the CD-0 Mission Need for the NSTX Upgrade Project was approved by the US Department of Energy Office of Science. During FY 2009 the conceptual design of the center-stack and NBI upgrade was carried out which culminated in a successful independent conceptual design review in October 2009. Features of the machine upgrade include; 1. a new toroidal field (TF) inner leg bundle including flags, hubs, and flexible connectors, 2. a new ohmic heating (OH) solenoid, 3. new upper and lower poloidal field (PF) coils PF1A, B, C, 4. new microtherm thermal insulation, 5. a new Center Stack Casing (CSC), 6. new plasma facing components (PFC) associated with CSC including the inboard divertor (IBD), and 7. a second beamline (BL) including the necessary structural, vacuum pumping and BL services. A successful Office of Science (Lehman) CD-2 review was conducted in August 2010 followed by an External Independent Review (EIR) in October 2010 which found the project ready to move forward with final design. DOE granted CD-2 approval in December 2010. A final design was conducted in June 2011 in preparation for a CD-3 (Critical Decision -3) Readiness Review. CD-3 approval was granted in December 2011, [2].

The NSTX upgrade outage started on Oct. 1, 2011, six months earlier than the original schedule due to the TF electrical short that occurred in FY 2011 on NSTX. After a review by a panel of external magnet experts, the lessons learned on the soft solder flux issue which led to the TF failure was incorporated into the NSTX center-stack upgrade manufacturing process to prevent similar failures for NSTX-U. This start of the upgrade outage offered an opportunity to accelerate the NSTX Upgrade Project schedule by up to six months. At the start of the outage, the NSTX diagnostics were carefully removed with proper documentation and were stored or shipped to the collaborating institutions as requested.

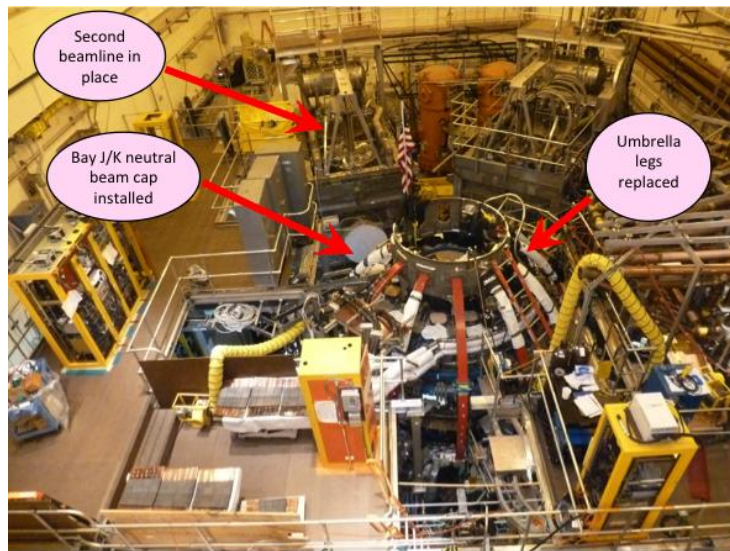


Fig. 10.8. An aerial view of the NSTX-U Test Cell with the 2nd NBI placed in its final position (March 2013).

After properly securing the NSTX facility, the NSTX operations technical staff was shifted to the Upgrade Project tasks as rapidly as possible. The NSTX technical staff also supported the NSTX-U infrastructure refurbishments including fault detector and firing generator for rectifier controls, migration of the plasma control system to modern processors, and reconfiguration of the Multi-Pulse Thomson Scattering (MPTS)

system. The NSTX technical staff also supported outgoing collaboration activities including lithium granular injectors and droppers on EAST, RFX, and DIII-D. The NSTX Upgrade Project has made excellent progress in FY 2012. The existing center-stack and associated components have been removed from the NSTX device. The Upgrade Project activities ramped up rapidly in all areas and are currently on pace to be completed in the summer of 2014 well ahead of the Sept 2015 CD-4 completion target date. The recent NSTX-U Test Cell aerial view taken in March 2013 is shown in Fig. 10.8. To provide capabilities needed to carry out the NSTX-U scientific research, the NSTX Team identified high priority facility and diagnostic enhancements for post upgrade operations. These include diagnostics provided by NSTX Research Team members from U.S. laboratories other than PPPL. To facilitate the planning process, facility and diagnostic enhancement brainstorming meetings were held and many innovative ideas were proposed. A theory brainstorming meeting was also held, and this motivated discussion on future experimental opportunities and associated facility and diagnostic needs.

10.3.1. New Center Stack Upgrade

The new center-stack part of the NSTX Upgrade Project has multiple elements including the fabrication of the new center-stack (10.3.1.1), the structural enhancements to the device for the ~ 4x increased electromagnetic forces (10.3.1.2), and the associated sub-system enhancements to supported the doubling of the TF current and 5 sec plasma pulse length (10.3.3).

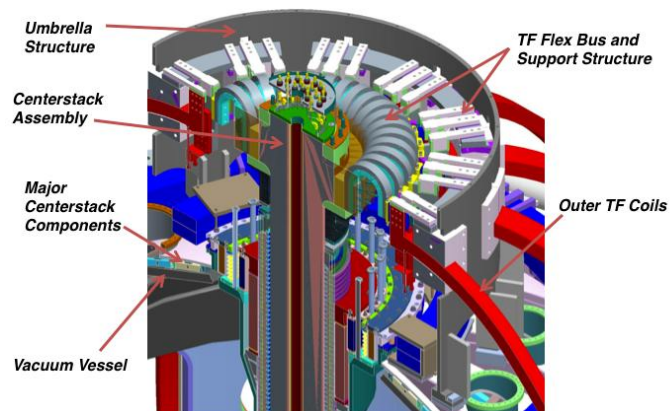


Fig. 10.9. A general arrangement drawing of upper umbrella structure area including the center-stack and TF Flex bus and associated support structure.

10.3.1.1. New Center Stack Fabrication

A general arrangement drawing of the upper umbrella structure area is shown in Fig. 10.9. The new center-stack is connected to the outer TF through 36 U-shaped TF Flex Buses. A more detailed the center-stack drawing is shown in Fig. 10.10 (a). The NSTX Upgrade Project has begun work on the critical path fabrication of the center-stack (CS) components including friction stir welding of lead extensions to the inner TF conductors.

The procurement of critical and long lead items are being carried out including the center stack plasma facing components, inner PF coils, the center-stack casing, and other TF/OH materials. During FY 2011, the design of the center-stack components including the Ohmic heating coil, inner TF bundle, Inner PF coils and the Center-stack casing was completed. The TF flex-bus is an important component to handle the TF current (130 kA) for about 7 sec while the accommodating the vertical growth of inner TF coil conductor of ~ 1cm and the electromagnetic forces. The TF flex-bus as shown in Fig. 10.10 (b) was successfully manufactured using EDM process and tested for 200,000 cycles which is more than three times the pulse cycle requirement. In FY 2012, the center-stack fabrication has started. NSTX technical staff have also set up in-house manufacturing facilities for soldering the TF cooling tubes and manufacturing of the OH and TF coils. A number of purchase orders and contracts have also been issued. These include:

- 1) Copper conductor for the Inner TF, OH and Inner PF coils were placed and they have been received. The Inner PF copper has been completed and has been shipped.
- 2) The machining and Friction-Stir-Welding operations for joining the joint section with the Inner TF conductor was awarded to Major Tool. All of the 36 inner TF conductors needed for making up the full TF bundle

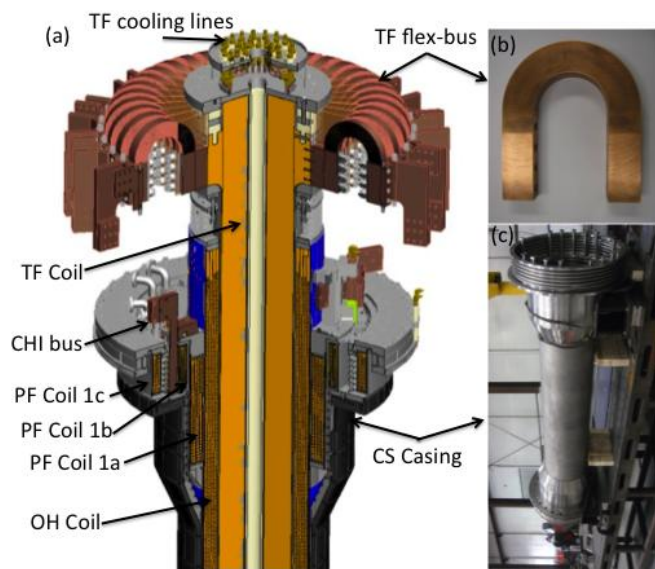


Fig. 10.10. (a) A schematic of the new center-stack and the TF joint area. (b) Fabricated flex-bus. (c) Fabricated center-stack casing.

flex-bus as shown in Fig. 10.10 (b) was successfully manufactured using EDM process and tested for 200,000 cycles which is more than three times the pulse cycle requirement. In FY 2012, the center-stack fabrication has started. NSTX technical staff have also set up in-house manufacturing facilities for soldering the TF cooling tubes and manufacturing of the OH and TF coils. A number of purchase orders and contracts have also been issued. These include:

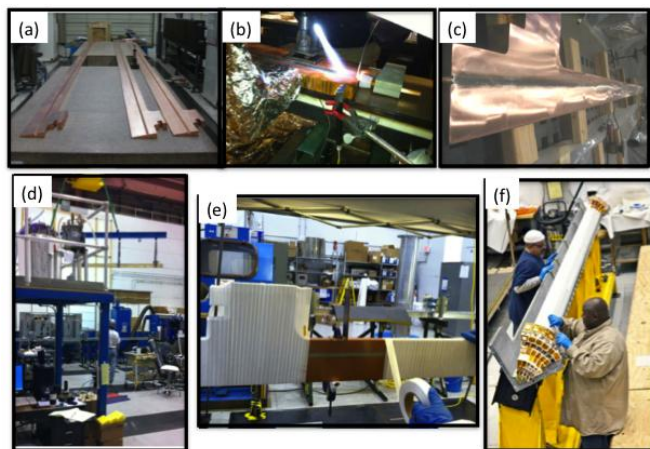


Fig. 10.11. The inner TF bundle manufacturing stages. (a) Machined conductor, (b) Cooling tube being soldered into conductor, (c) Conductor after cooling tube installation and grinding, (d) Conductor being removed from oven after sandblasting and priming, (e) Conductor being wrapped with fiberglass insulation, and (f) Insulated conductor being placed into mold.

were received along with a few spare conductors.

- 3) The contract for the Inconel Casing was delivered in December 2012 as shown in Fig. 10.10 (c). And
- 4) Requisition for the Inner PF coils and structure is ready for procurement.

The TF bundle manufacturing stages are shown in Fig. 10.11. During this past year, PPPL has developed the methodology for soldering the cooling tube into the Inner TF conductors without use of the zinc chloride based flux which caused the original TF bundle failure. The soldering operation for a full bundle has been completed. The coil fabrication area has been setup and is fully functional. The inner TF conductors for 3 quadrants have been sandblasted, primed and insulated. The insulated conductors are installed into the quadrant mold for Vacuum Pressure Impregnation (VPI) with CTD-425 (Cyanide-Ester Blend Hybrid) as shown in Fig.10.11. The first quadrant was successfully VPI'd as shown in Fig. 10.12 in early March 2013 and it passed the electrical test. Following the first VPI, the VPI for the balance of quadrants will be performed at a pace of about one quadrant per month. Once the individual Quadrants are VPI'd, the full TF bundle will be VPI'd. Then the winding of the OH coil over the full TF bundle will be performed followed by a VPI of the entire TF-OH center-bundle. In parallel, the completion of the Center-Stack Casing will begin this spring with the welding of the 700 inconel studs for mounting the carbon tiles to the walls. The carbon tiles (PFC) will then be mounted with surface diagnostics to the casing walls. Once the inner poloidal field (PF) coils arrive, they will also be joined to the casing as shown in Fig. 10.10. The completed OH/TF bundle and CS casing will be transported to the NSTX-U for final assembly. Delivery of the completed CS Assembly is scheduled for Spring 2014.

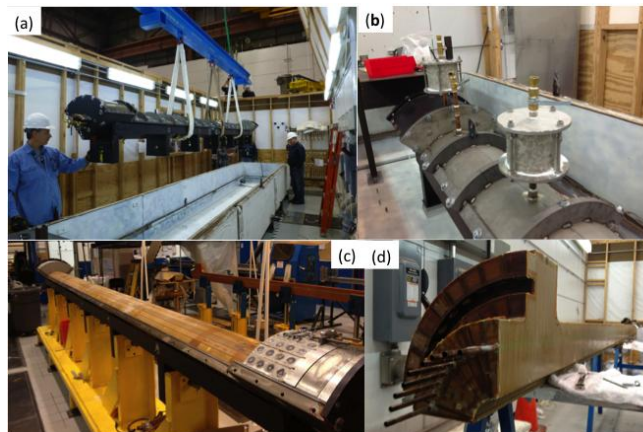


Fig. 10.12. TF Quadrant VPI. (a) TF Quadrant VPI mold lowered into the oven. (b) TF Quadrant VPI mold readied for VPI. (c) and (d) TF Quadrant after VPI.

10.3.1.2. NSTX-U Device Structural Enhancements

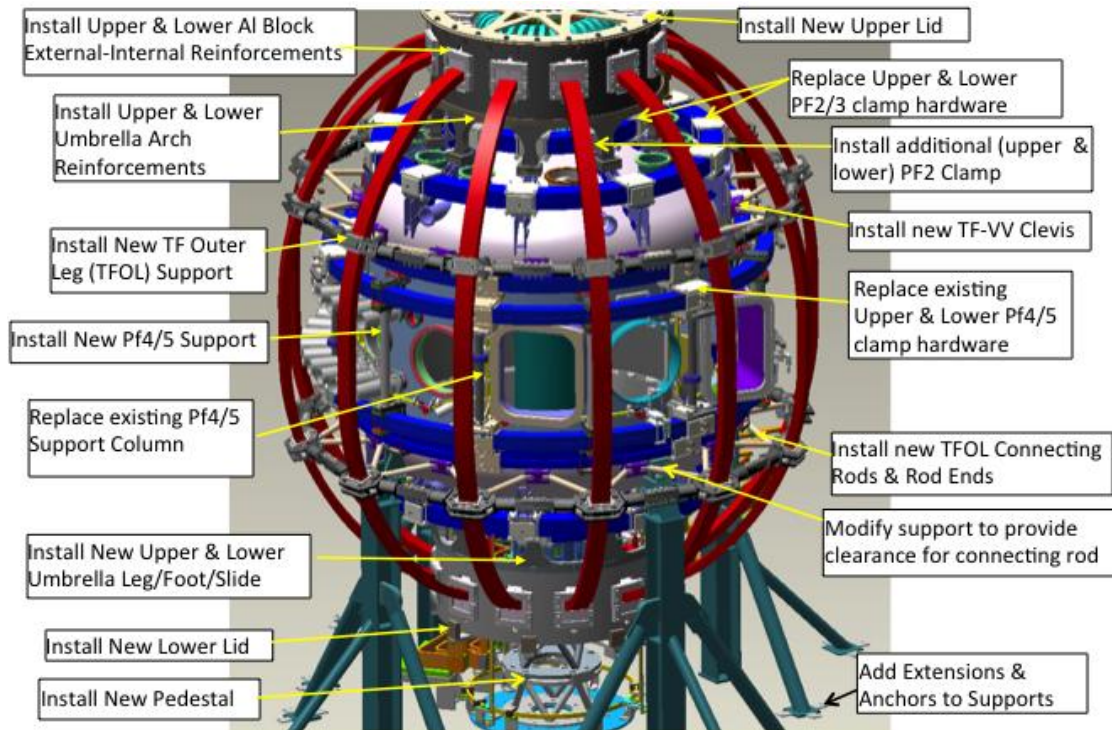


Fig. 10.13. NSTX-U support structural upgrades

I

In order to handle the anticipated 4x greater electromagnetic forces for NSTX-U, the vacuum vessel and associated magnetic field coil support structures must be enhanced accordingly. During FY 2011, the drawing details were completed for the Vacuum Vessel (VV), outer TF coil, PF coil, and passive plates support upgrades. The planned device structural upgrades are illustrated in Fig. 10.13. Procurements were placed for the fabrication of the umbrella structure reinforcements, PF 2/3 support upgrade hardware and PF 4/5 support upgrade hardware. The outer TF leg support upgrades were also fabricated. The TF-VV clevises to better support outer TF legs were welded onto the vessel. The new umbrella legs were installed on the machine.

The vacuum vessel leg attachment connections were modified to clear the clevises. In addition, since the plasma disruption forces are also expected to also increase by a factor of 4, the internal passive plates were reinforced by replacing the stainless steel attachment hardware with Inconel versions. The support structure enhancement activities are ongoing. Some photos of the support structure enhancements are shown in Fig. 10. 14.

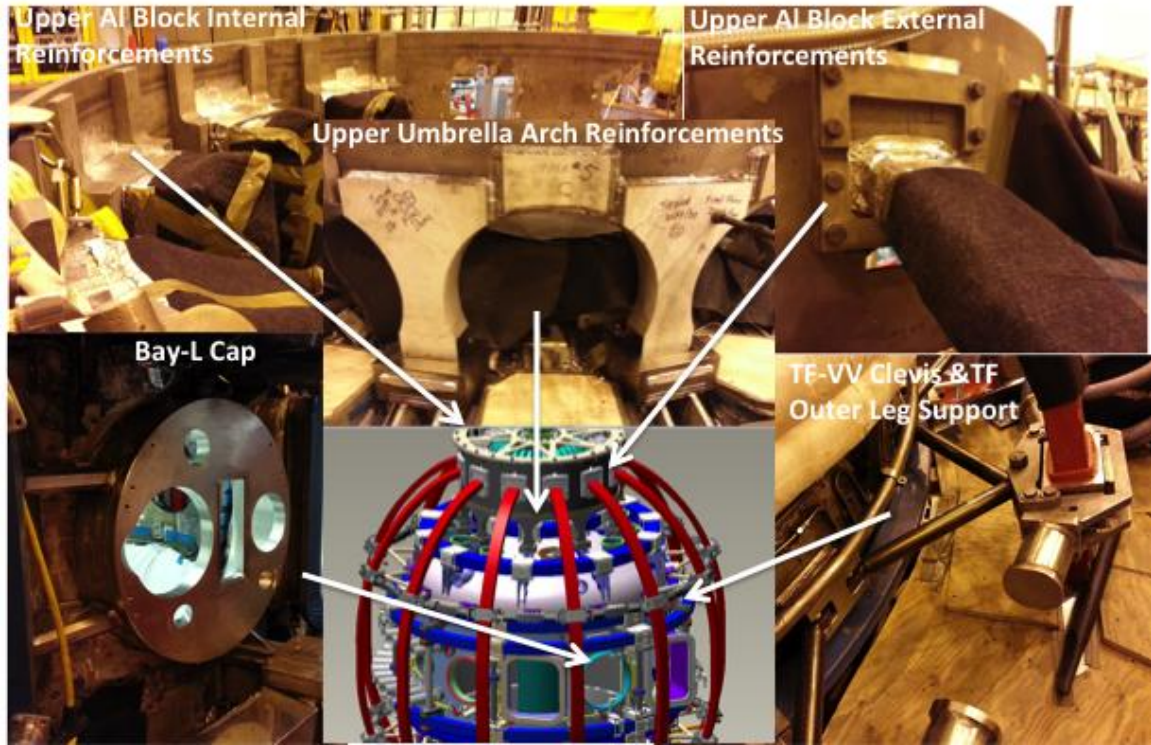


Fig. 10.14. NSTX-U support structural upgrades photos (March 2013).

10.3.2. Second Neutral Beam Injection System Upgrade

The 2nd NBI upgrade scope is to add a complete, functional second beam-line (BL) to NSTX-U at aiming tangency radii of 110, 120 and 130 cm compared to 60, 70, 80 cm for the 1st Present NBI as shown in Fig. 10.6. This task largely utilizes the existing TFTR NBI infrastructure. The 2nd NBI tasks include the TFTR NBI BL tritium decontamination, refurbishments, sources, relocation, services, power and controls, and NTC arrangements, as well as Vacuum Vessel modifications, the NBI and TVPS Duct, and NBI armor. The general drawing of the NSTX-U Test Cell with the 2nd NBI system is shown in Fig. 10.7. Decontamination of a TFTR BL began in 2009 and was deemed complete such that the BL was acceptable for use on NSTX. Refurbishment of the BL includes box, lid and cryopanel, ion dump, 90 inch flange, calorimeter, magnet, and shields, and the source platform and peripherals. Relocation involved a series of steps to make way for the BL from TFTR Test Cell (TTC) to South High Bay into the NSTX-U Test Cell (NTC) as well as the discreet equipment moves. The ion source refurbishment job has been completed and closed. The BL decontamination (decon) was performed in the TTC with full disassembly of TFTR BL4, inspection and refurbishment of components. The decon job was completed and closed. BL relocation began in September 2012. The BL box and lid were moved into the NTC and reassembled as shown in Fig. 10.15. The installation of the support structure and alignment of the BL has been completed as shown in Fig. 10.16. The refurbished 90 inch flange, ion dump, calorimeter, and bending magnet shown in Fig. 10.17 were installed on the BL. The source platform has been fully decontaminated and installed. The latest 2nd NBI view can

be seen in the recent (March 2013) test cell aerial view shown in the chapter heading. Relocation also includes moving three High Voltage Enclosures (HVEs) from the TTC Basement into the NTC also. The HVEs have been prepared for removal. The pathways through the areas have



Fig. 10.15. Relocation of the 2nd NBI beam line box. (a) The beam box lifted over the NSTX-U Test Cell. (b) The beam box being lowered into the final position in the NSTX-U Test Cell. (c) The beam box being assembled.

been cleared. When the BL components have been removed from the TTC and the floors decontaminated, the HVEs will be brought up to the TTC floor and taken into the NTC. This work is planned for 2nd quarter FY13.

The BL services include water, vacuum, Liquid Nitrogen (LN) and Liquid Helium (LHe) cryogenics, SF₆, feedstock gas, and pneumatics. Progress includes the fabrication and installation of the LN manifolds in the NTC up to the BL, fabrication of LHe lines and valve manifolds in the NBI shops. Penetration drilling in the NTC floor for water system piping and in the NTC West wall for LHe cryogenics piping has been completed.

A water system installation package is in development for a requisition and subcontract planned for later this fiscal year. Power system progress includes the preparation of specification and purchase of all major cabling required to fully connect the N4ABC power systems from the TFTR area to the NTC location via the TFTR Test Cell Basement.

The major high voltage cabling triax has been manufactured, delivered and successfully tested on site. A power cable and tray procurement package is being prepared for installation of tray and cable pulls to connect the power supplies. This subcontract will be awarded and cable and tray installed beginning later this FY 2013. The penetrations required in the NTC West wall have been completed for all of the power cabling.

Major progress on controls may be noted. Racks have been installed in the gallery area and populated with chassis electronics to control both BL1 and BL2. The Local Control Centers for N4ABC have been addressed to add NI electronics and LabView software controls. Power supply controls have been updated in the Switchyard, Surge Rooms, Mod/Regs, and Decels. Three Gradient Grid Dividers have been fabricated for the Mod/Regs. Progress continues on LCCs.



Fig. 10.16. 2nd NBI alignment performed and confirmed.

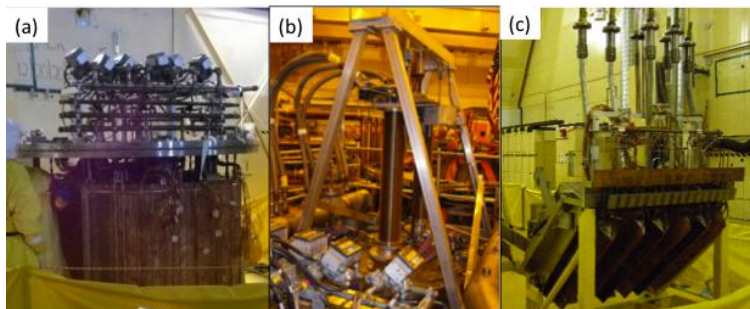


Fig. 10.17. Beam-line component refurbishment. (a) Ion Dump replacement reassembly in progress. (b) Calorimeter upgrade with double bellows – double drive in progress. (c) Bending Magnet ready for installation.

Fabrication of the NBI armor to be located inside the VV is in progress. The carbon tiles have been machined. The backing plates have been fabricated. The assembly and brazing are planned later this month in the shop. Supports have been tack welded in the vessel and will be checked with the backing plates. A Bay H port cover has been for the water and thermocouple feedthroughs. Final

welding, assembly, and installation of the NBI armor was completed for January 2013. The Duct and VV modification at Bay JK has been completed. A new Bay JK “bay window” or cap was required for accommodating the strongly tangential aiming angles. The NBI vacuum vessel modification is shown in Fig. 10.18.

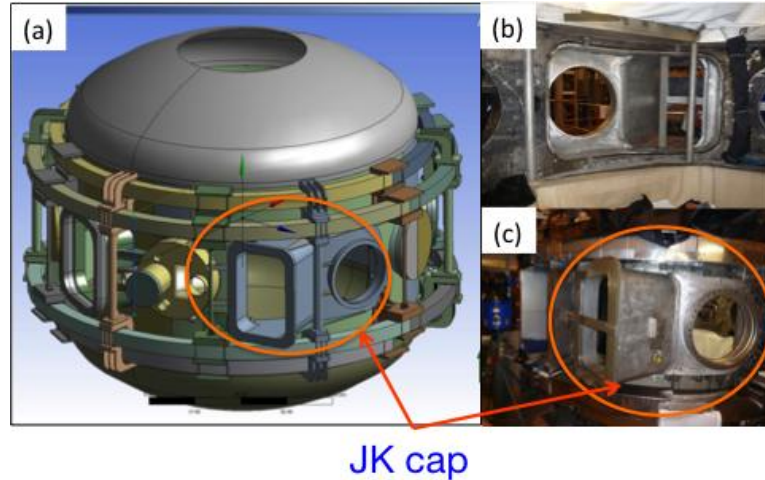


Fig. 10.18. NBI-related vacuum vessel modification (a) Modified vacuum vessel schematic. (b) Bay J-K bay window inside view. (c) Bay J-K bay window external view.

The opening for the new caps was cut on the VV and the welding of the new Bay JK and Bay J caps onto the VV has been completed. The rectangular bellows for the NBI duct has been fabricated and leak checked. The major flanges and structures for the duct have been fabricated or are in progress in the shops. Since the original vacuum vessel duct and the torus vacuum pump system (TVPS) located in Bay L were removed, the

TVPS was incorporated into the NBI transition duct for NSTX-U as shown in Fig. 10.19. The Torus Vacuum Pump System (TVPS) ducts have been fabricated. All procurements for the duct and TVPS are delivered. The large circular and rectangular bellows have been procured, manufactured, and

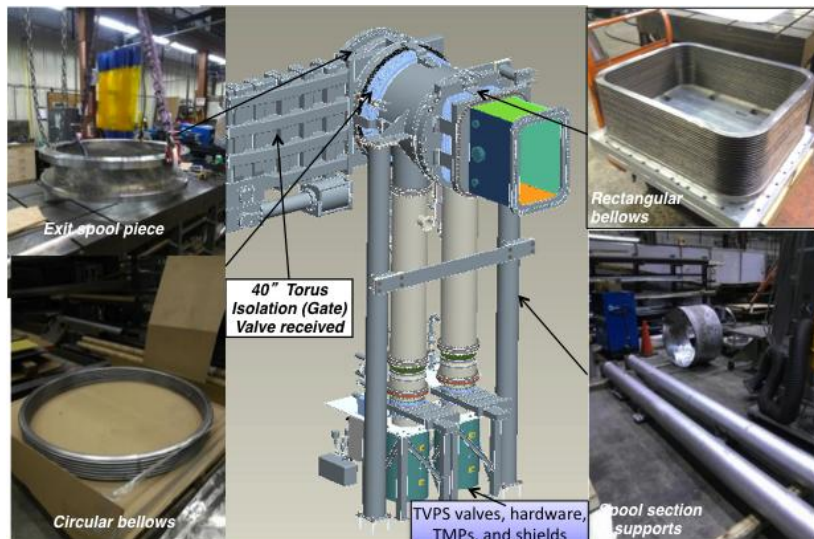


Fig. 10.19. NBI Duct and Torus Vacuum Pumping System (TVPS) components being procured and fabricated.

received. The Torus isolation Valve for the BL has been received. The NTC required extensive rearrangements to create the floor space for the BL. All rearrangements have been completed. New platforms have been installed. The TVPS racks have been moved to the gallery area. Diagnostics were removed and the Bay L pump duct was permanently removed. The BL has been located into its final position so reassembly of the locale is in progress and will continue for the rest of FY13.

With successful completion of the above tasks, preoperational testing of BL systems and N4ABC power and controls will be required to commission subsystems and confirm readiness for operations. This testing will begin in FY14 and flow into startup operations based on project baseline schedules and funding profiles.

10.3.3. NSTX-U Facility Subsystems

The NSTX TF, OH, PF1AU, PF1AL Power Systems are redesigned to meet NSTX Upgrade requirements. Other circuits remain the same. The re-design is done under space constraints of the NSTX power supply facility.

10.3.3.1. TF and OH Power Systems for NSTX Upgrade

NSTX Upgrade requires an increase in the TF field. Thus the TF feed was designed to a rating of 1kV, 129.8kA for 7.45 seconds every 2400 seconds. Also the design is such that the pulse period can be reduced to 1200 seconds in the future by providing additional power cabling in the power loop. The NSTX rating was 1kV, 71.2kA for 1.3 seconds every 300 seconds. To meet the upgrade requirements, four additional branches are added to the existing four branches. The existing four TF Safety Disconnect Switches (SDS) will be continued to be used with two parallel branches through each SDS. Extensive power cabling reconfiguration has been undertaken in the TF wing of Field Coil Power Conversion (FCPC) building. Ninety-six (about 6200 feet) TFTR-era cables are being disconnected, removed, and scrapped. Hundred of cables (about 5800 feet) are to be pulled and installed. Also additional cables from the Transition area to the NSTX test cell are to be provided for TF circuit. So far (as of March, 2013), about 70% of the installation work is completed.

New accurate fiber optic DCCTs (+/-150kA) will be provided to measure the TF current. The PF1A circuit is redesigned without the ripple suppression reactors, which were used with the previous PF1A coils. These ripple reduction reactors (the original PLT TF coils) will now be used in the upgraded OH circuit as the branch DC current limiting reactors (CLR) and the power cabling will be modified as needed. The existing OH power supply

is designed to have the capability of 6kV, +/-24kA and meets the new requirements based on PSCAD analysis.

A Digital Coil Protection (DCP) System is being designed and implemented. Protection system will be upgraded to meet the new requirements. Currently each circuit is protected from over-current, $I^2 \times t$, higher pulse duration, and higher than permitted pulse period. In the new scheme, the forces from a combination of current in coils will also be computed and additional protection accorded. The Hardwired Control System (HCS) is being upgraded with a PLC for the TF wing. A unique TF turn to turn short detection scheme has been designed using a fiber optic DC Current Transducer (DCCT). In this scheme a fiber sensor will be installed towards the top of the machine and will interleave the 12 TF bundles detecting the differential current which will be normally zero. In the event of a fault the DCCT will detect a current and the circuit will be tripped.

10.3.3.2. Rectifier Control System Upgrades

The Transrex AC/DC Convertors of the NSTX Field Coil Power conversion System (FCPC) provide a pulsed power capability of 1800 MVA for 6 seconds every 300 seconds. The modular converter concept of 74 identical, electrically isolated 6-pulse “power supply sections” was originally used on TFTR as shown in Fig. 10.20, and then adapted to NSTX which has a more complex topology including anti-parallel and three wire configurations. In order to extend the useful operational life of this system, which has remained largely unchanged since 1984, it is necessary to replace key elements of the FCPC controls. The elements to be redesigned and replaced are the Firing Generators, the Fault Detectors, the electromagnetic relays which provide the interlock logic in the “Hardwired Control System (HCS)”, and the HCS to Fault Detector interface.



Fig. 10.20. Photograph of the FCPC facility.

The rationale for this refurbishment is based on the facts that many parts are nearing end-of-life due to age and wear, replacement parts are rare or unavailable, and that

performance can be improved to the NSTX-U requirements using more modern control equipment. Precise control of thyristor firing angles by the FCPC firing generators has always been necessary for NSTX operations, and becomes more critical for the new 8-parallel, 130kA TF system configuration. In addition, the ability to separately control the “A” and “B” sections of each power supply unit allows for more efficient utilization of the 74 available sections. The new Firing Generator (FG) is the highest priority task and, compared to the original FG, will deliver firing pulses with far greater resolution, precision, and repeatability, and can receive and process separate commands to the A and B sections as noted above. The prototype FG has been fully tested in a Transrex rectifier, and production units are being fabricated. The new Fault Detector (FD) provides the same functionality as the existing FD in terms of faults detected, but includes an improved external interface compatible with the present NSTX data acquisition system. The implementation of the new FD is considered a lower priority than the FG, but testing of the FD prototype has been completed in conjunction with the new FG in a Transrex rectifier.

The electromagnetic relay logic in the Hardwired Control System (HCS-Relays) is being replaced with PLC-based interlock logic. This will provide enhanced reliability via the elimination of old electronic devices, and will provide an interface to the NSTX data acquisition system which will indicate the status of all interlock logic criteria. A further improvement to the system involves the implementation of PLC compatible I/O modules to each Transrex power supply, interfacing the new FD, and connecting to the PLC in the HCS control board (HCS-FD). This feature provides a redundancy to the existing HCS fault logic, and includes the ability to see the status of each individual power supply in the loop.

10.3.3.3. Poloidal Field Coil Power Supply Upgrades

The NSTX-U Upgrade will have three PF 1 coils, PF 1A, 1B, and 1C for both upper and lower divertor regions as shown in Fig. 10.21. The new upgraded configuration would allow improved divertor configurational control and up-and-down symmetric configurations. The first-year power supply capabilities of NSTX-Upgrade will yield considerable experimental flexibility. For instance, by powering the PF-1A & Bipolar PF-1C upper and lower supplies,

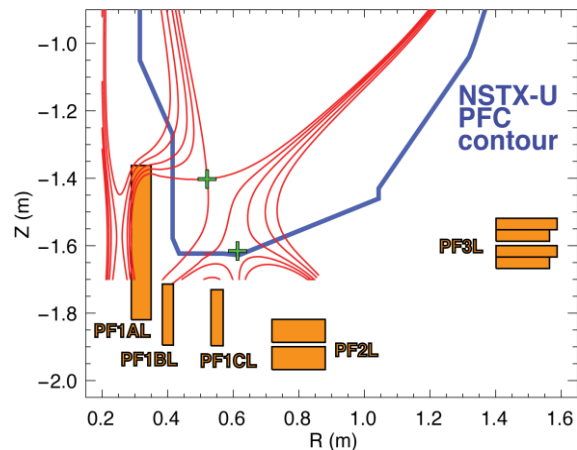


Fig. 10.21. A schematic of lower PF 1A, B, C, 2, & 3 coils in NSTX-U.

it will be possible to generate up-down symmetric snowflake divertors in NSTX-U, a capability that did not exist in NSTX. This upper and lower PF-1A and Bipolar PF1-C capability also facilitate the coaxial helicity injection current start-up research (10.5.3.1). Longer-term, the following potential upgrades to the power supply systems may add considerable new capability: The PF-2 coils, currently configured for unipolar operation, may be upgraded to bipolar operations. This will allow those coils to either create the snowflake divertor or to control the lower plasma-wall gap in the high-triangularity shapes, without changes to the power supply links. The PF-1B coil will not be powered during initial upgrade operations. However, calculations have indicated that this coil may be important for maintaining a steady snowflake divertor through the full OH swing, and that coil will be powered if this deficiency is found to be significant for operations. In future PF5 is also proposed to be upgraded to carry 34kA as compared to the existing level of 24kA.

10.3.3.4. Migrate Plasma Control System to Modern Processors

A substantial upgrade to the NSTX-U plasma control system infrastructure is occurring in parallel with the Upgrade construction activity. A new 32-core control computer has been acquired. This computer, provided by Concurrent Computer Corporation, uses the Red Hawk operating system, a version of Red Hat Enterprise Linux customized for real-time applications and equipped with numerous advanced real-time debugging and testing features. The new computer has four input data streams which, along with upgrades to the digitizers used for acquisition, will allow the sampling rate for real-time data acquisition to be increased from 5 kHz to ~25 kHz. Finally, the TFTR-legacy system for sending commands to the PF & TF coil power supplies has been updated, eliminating one of the slowest sections of the real-time data and control stream. As the date for NSTX-U operation nears, a second real-time computer will be acquired, providing a backup for NSTX-U operations and allowing parallel testing of control code during NSTX-U operations.

10.4. RF Heating and Current Drive Systems

The NSTX RF heating and current drive (CD) systems will consist of the existing 6 MW high harmonic fast wave (HHFW) system [3] and the new ECH/EBW system, which is an important element of the NSTX five year facility upgrade plan. The HHFW system is expected to perform better with higher toroidal field of NSTX-U. After the initial HHFW operation with the NSTX-U plasmas, an upgrade of the HHFW antennas is envisioned to increase the heating power and heating / CD efficiency. The ECH/EBW system is particularly crucial for the non-inductive start-up research where it can be effectively

bridge the temperature gap between the CHI based start-up plasmas which tends to be below 50 eV and the HHFW heating and CD regime which tends to be above ~ 200 eV. It is estimated that about 0.5 to 1 MW to ECH/EBW power would be sufficient to heat the CHI plasmas to ~ 200 eV range. The ECH/EBW system could also provide an efficient off-axis CD needed for advanced ST operations.

10.4.1. HHFW Upgrades

In the HHFW area, while the system is basically unchanged, the HHWF feed-thru conductor must be modified to be able to handle the higher disruption loads ($\sim \times 4$) in NSTX-U. The HHFW antenna installed in NSTX is shown in Fig. 10.22. To handle those disruption loads, compliant connectors will be designed, tested and installed between the feed-throughs and antenna straps for the NSTX-U operations. A HHFW poloidal limiter upgrade to handle higher power and longer pulse NBI

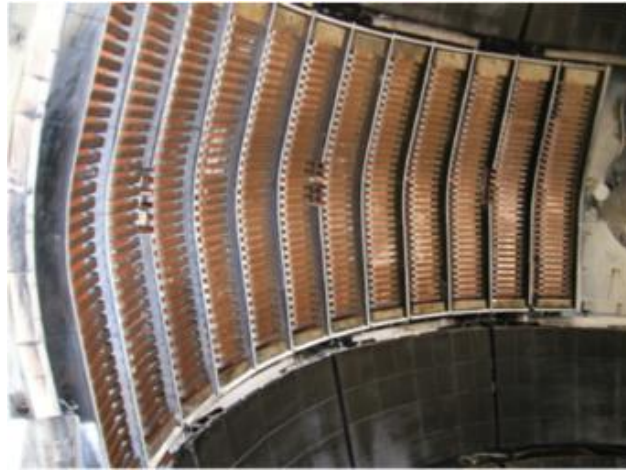


Fig. 10.22. Photograph of the HHFW antenna in NSTX.

power will also be considered once the power handling requirements are obtained during the initial NSTX-U operation. In order to increase the power from the existing 12-strap HHFW antenna, RF voltage stand-off tests will be conducted on an RF test stand in FY2013-14. These tests will allow the determination of the location of RF-induced arc-prone areas so that those weak areas can be modified to achieve higher voltage stand-off. These tests will also determine if the feed-through geometry needs to be modified to achieve a higher stand-off voltage. During HHFW operations on NSTX lithium compound dust entered the HHFW antenna resulting in significant antenna arcing that limited the maximum arc-free power that could be coupled to the plasma. To mitigate this problem a double Faraday shield will be considered. If budgets permit, the RF source controls will be upgraded on sources 3 and 4 from the existing relay control system to a modern programmable logic controller (PLC) system. The RF source 1 and 2 controls will also be upgraded to a PLC system at lower priority. This should lead to a significant improvement in source reliability.

In order to provide space for the ECH/EBW launcher and antennas that can couple to edge harmonic oscillations (EHO) and/or Alfvén eigenmodes, it is possible that four of the HHFW antenna straps would be eventually removed. With improvements in antenna

voltage stand-off hoped for with the RF test stand and the reduced lithium-induced arcing resulting from installation of the double Faraday shield discussed above, it may be possible to couple sufficient HHFW power with only 8 antenna straps. Before removing the straps the 12-strap antenna will be temporarily configured for 8-strap operation so that 8-strap operation can be evaluated in NSTX-U.

10.4.2. Electron Cyclotron / Electron Bernstein Wave Heating System

A 28 GHz high-power electron cyclotron/electron Bernstein wave (EC/EBW) heating system is planned for installation on NSTX-U. Assuming the baseline (or incremental) budget this system will be installed in 2017-18. Initially this system will provide electron heating during non-inductive plasma start-up, later it will be used for off-axis EBW heating and current drive [4]. EC modeling of a CHI start-up plasma predicts significant first pass absorption even at the relatively low core electron temperatures that

were typical of CHI plasmas in NSTX. For EC heating of under-dense start-up plasmas a fixed corrugated horn launcher will launch extraordinary mode (X-mode) 28 GHz power. In order to heat over-dense start-up discharges at 28 GHz a double mode conversion scheme will be employed to excite EBWs in the plasma. The scheme will use a grooved graphite mirror polarizer tile on the center column of NSTX-U to mode convert ordinary mode (O-mode) power incident from the low field side of NSTX-U, into X-mode power. The X-mode power reflected from the polarizer propagates back to the plasma, passes through the EC resonance (ECR) layer and undergoes a subsequent X-mode to EBW mode conversion near the upper hybrid resonance (UHR) layer. Then the excited EBW mode is totally absorbed before it reaches the Doppler-shifted ECR layer.

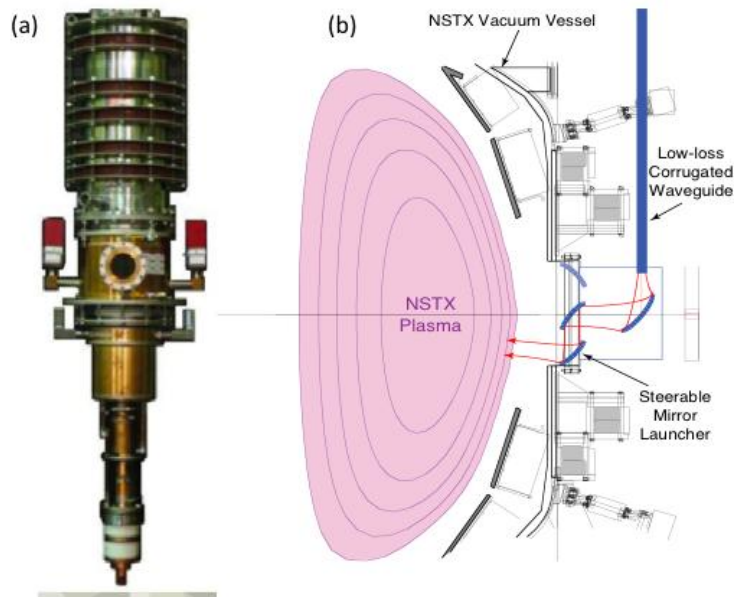


Fig. 10.23. NSTX-U ECH/EBW System. (a) 28 GHz – 1MW gyrotron tube by U. of Tsukuba. (b) A schematic of the NSTX-U ECH/EBW launcher

The EC/EBW heating system will use a 28 GHz gyrotron originally developed for EC heating in the GAMMA10 tandem mirror [5]. The gyrotron as shown in Fig. 10.23(a) has an output power of ~ 1 MW, a pulse length of up to 5 s and uses a $TE_{8,3}$ cavity mode. The gyrotron will be powered by a modified TFTR neutral beam power supply located in the former TFTR test cell located next to NSTX-U. The 28 GHz power will be transmitted to NSTX-U via low-loss, 50 mm diameter, corrugated $HE_{1,1}$ waveguide. Initially the 28 GHz heating system for heating start-up discharges. Later, when the system is used for off-axis EBW heating and current drive studies during the plasma current flattop, and the gyrotron power will be increased to 2-4 MW. A schematic of the ECH/EBW launcher is shown in Fig. 10.23 (b). Coupling to the EBWs in the plasma will be accomplished via O-mode to slow X-mode to EBW (O-X-B) double mode conversion. An actively-cooled, concave steerable mirror launcher will focus the 28 GHz power on the EBW mode conversion layer. To generate EBW current drive, in addition to EBW heating, the focal spot will be poloidally offset from the mid-plane to introduce an up-shift in parallel wave number in the plasma.

10.5 Facility Science Tools

10.5.1. Macro-stability Tools

While NSTX-U is a modification of NSTX, changes to the device conducting structure (e.g. new 2nd NBI port structure), mid-plane RWM control coils, and equilibria require re-computation of $n = 1$ active RWM control performance using proportional gain, and RWM state space control. The upgrade also adds new capability, such as independent control of the 6 RWM coils. The base NSTX-U 3-D MHD control coils and magnetic sensor are shown in Fig. 10.24 [6]. This new capability, combined with the upgrade of the RWM state space controller will also allow simultaneous $n = 1$ and $n = 2$ active control, along with $n = 3$ dynamic error field correction. Finally, the active control performance of the proposed off-mid-plane non-axisymmetric control coils (NCC) [6] also needs to be evaluated. A significant increase in controllable \square_N is expected with the RWM state space control in NSTX-U, as was found for NSTX.

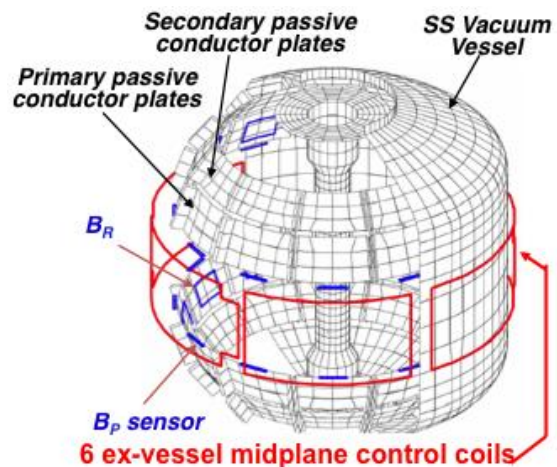


Fig. 10.24. 3-D MHD control coils and magnetic sensors.

10.5.1.1. 2nd Switching Power Amplifier (SPA)

An additional 3-channel Switching Power Amplifier was installed and commissioned in FY2011. With this addition, six SPA channels will allow each of the six non-axisymmetric radial-field perturbation coils (Fig.10.24) on NSTX-U to be powered independently, thereby providing the capability for simultaneous control of the toroidal harmonics, $n = 0 - 3$, of the applied field perturbations. The power testing of the rectifier and DC power link from the FCPC power supply hall was completed in March, 2011. Following pre-operational testing of the system and the incorporation of changes to the NSTX power supply controller to accommodate the additional SPA commands in its output stream, operation of all six SPA channels powering their respective error-field control coils was achieved in July, 2011. The basic software modifications to the higher-level Plasma Control System (PCS) software for operating and controlling the second SPA were then installed and independent programmed control by the PCS of the currents in the six error-field correction coils was demonstrated. This capability should be available for the Day-1 NSTX-U operation.

10.5.1.2. Non-axisymmetric Control Coils

Recent RWM stability calculations have been performed for NSTX-U using an expanded non-axisymmetric coil set similar to one originally proposed for NSTX [6]. The proposed non-axisymmetric control coil (NCC) will enable us to explore such variability and utility of 3D field applications, with much

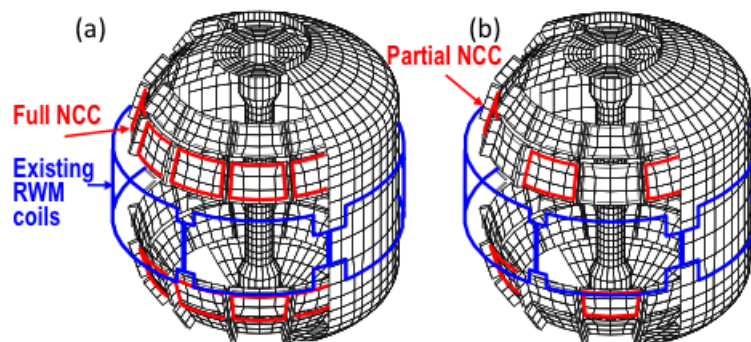


Fig. 10.25. Non-axisymmetric Control Coils shown in red. The existing error field coils are shown in blue. (a) Full NCC Option with 12 x 2 coil arrays. (b) Partial 6 x 2 NCC Option for incremental installations.

wider and unprecedented flexibility of field spectrum in space. In Fig. 10.25, schematics of possible NCC configurations are shown. The full toroidal NCC array (2 x 12) shown in Fig. 10.25 (a) has 12 coils in the upper and lower primary passive plate positions (see Fig. 10.24) and it is chosen to generate high toroidal harmonic perturbations up to $n = 6$, and also up to $n = 4$ rotating fields. Because of limited resources, it might be necessary to implement the NCC system in stages. A reduced coil set NCC (odd 2x6) is shown in Fig. 10.25(b) with 6 coils each instead. While the n number is reduced to up to 3 for the

reduced set, it can still provide essential NTV, RMP, and EF selectivity with flexibility of field spectrum as synergy with the existing 3-D/EFC system. The implementation of the NSTX-U NCC coils is expected to benefit from the experience gained from the internal control coil system on DIII-D.

10.5.1.3. Disruption Mitigation Systems

A key issue for ITER, and the tokamak/ST line of fusion devices in general, is the avoidance and mitigation of disruptions. Most of the disruptions are expected to be mitigated by massive gas injection (MGI) as described in 10.5.1.3.1 [7]. For some disruptions, the warning time may be less than 10ms. At present there is no suitable disruption mitigation system that can deliver the required impurities to the core plasma on this timescale after an imminent disruption (with a warning time of < 10 ms) is detected. For mitigating those specially fast disruption events, an electromagnetic particle injector (EPI) is proposed as described in 10.5.1.3.2.

10.5.1.3.1. Massive Gas Injection

In order to investigate Massive Gas Injection (MGI), the most promising method found thus far for safely terminating discharges in ITER, the University of Washington team installed and commissioned high-capacity gas injectors at two different poloidal locations on NSTX-U. With these, NSTX can offer new data by injecting gas into the private flux and lower x-point regions to determine if this is a more desirable location for massive gas injection. By comparing gas injection from this new location to results obtained from a similar amount of gas injected from the conventional outer mid-plane, NSTX-U can provide additional insight, new data for improving computational simulations, and additional knowledge to understand disruption mitigation physics. For Massive gas injection

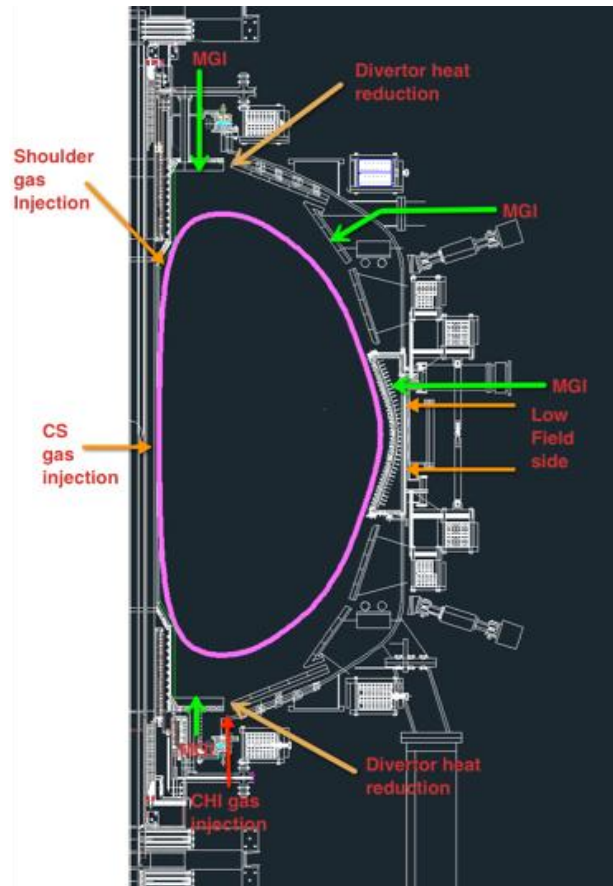


Figure 10.26. A schematic showing the various gas injection locations on NSTX-U.

studies, NSTX-U had the capability for injection from the lower divertor and from the mid-plane. In addition to these two locations, we will increase the poloidal injection locations (over a period of two years) to include a third location from the upper divertor and a fourth location from the upper primary passive plate region, as shown in Fig. 10.26. In addition, work is underway to improve the gas valves to provide faster gas throughput capability and reduced total amount of injected gas. This is based on recent results from DIII-D, C-MOD and ASDEX-U that indicate that only the gas injected within the first ms is efficiently assimilated by the plasma discharge.

10.5.1.3.2. Electromagnetic Particle Injector (EPI)

NSTX-U plans to test a novel mitigation technology referred to as the Electromagnetic Particle Injector (EPI). The system, propels a coaxial projectile, containing particulate matter of various sizes and composition, in a coaxial electromagnetic rail gun, then shatters it in order to inject the smaller sized particles into the tokamak. While experiments on NSTX-U would likely shatter the pellet, the system for ITER may choose to inject the capsule intact. The advantages of this system are that it can respond and deliver the impurity particles to the plasma core in much less than 10ms and that the system is well suited for long stand-by mode operation with high reliability. There are two components to this system. These are the injector itself and the power supply needed to drive the injector. Design studies of an injector for NSTX-U have converged on an attractive design, which results in a simple, compact injector. The injector measures about 12 inches in length and can be mounted on a 6-inch diameter port. The high cost component of the EPI system is the driving power supply, which must deliver about 150 kA of current for 0.5ms. Interestingly, the capacitor power supply used on NSTX-U to drive the CHI system is well suited to drive the EPI injector as well. During EPI system operation the coaxial current feeds that connect to the CHI bus bars will be disconnected from the NSTX-U machine and connected to the EPI injector. The EPI system is described in detail in Section 2.2.2.3.3.

10.5.1.3.3. Compact Toroid Injection

A system based on Compact Toroid Injection (CT) system has the potential for runaway electron suppression. On NSTX-U runaway electrons can be created during inductive start-up by maintaining a low vessel neutral pressure. Steady-state Advanced Tokamak (AT) scenarios and Advanced ST scenarios will rely on optimized density and pressure profiles to maximize the bootstrap current fraction. Under this mode of operation, the fuelling system must deposit small amounts of fuel where it is needed, and as often as needed, so as to compensate for fuel losses, but not to adversely alter the established density and pressure profiles. CT fuelling has the potential to meet these needs, while

simultaneously providing a source of toroidal momentum input. NSTX-U has access to a single pulse CT injection system that could be used for these studies. However, present priorities and budget levels would not allow these to be tested during the present 5 year plan.

10.5.2. Boundary Physics Tools

The base line PFCs for the initial NSTX-U operation is graphite tiles. The vacuum vessel interior with carbon tiles is shown in Fig. 10.27(a). Because of the increased plasma heat loads due to the increased NBI heating power and pulse duration, it was decided to enhance the protection of the CHI Gap. “CHI Gap” is the region between the NSTX-U inner and outer vacuum vessels, above or below the CHI insulators. As indicated in Fig. 10.27,

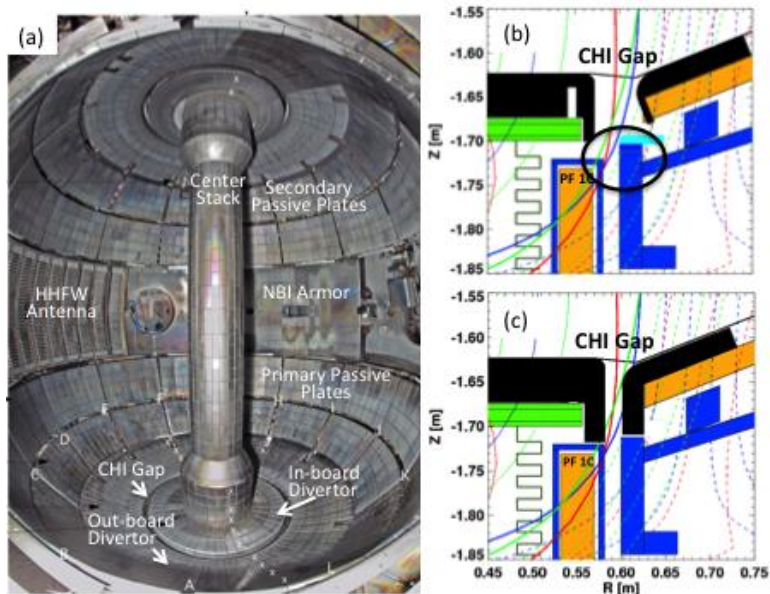


Fig. 10.27. (a) NSTX in-vessel view. (b) CHI gap view with NSTX gap tiles. (c) CHI gap view with new gap tiles for NSTX-U.

there is a gap in the graphite PFCs in the divertor region, resulting in exposure of the stainless steel and PF 1C to the plasma as shown in Fig. 10.27(b). Also because of the new PF 1C coil, which is placed in the CHI Gap region, an improved protection was deemed necessary. Control room observations showed that when the strike-point was placed in this region, severe contamination of the plasma could occur. This problem was anticipated to be much more severe in NSTX-U, where the horizontal inner target is narrower by a factor of two. Hence, as shown in Fig. 10.27(c), the graphite tiles on both the inner and outer divertors will be extended downwards, coming in close contact to the PF-1C coil casing and stainless steel outer vessel flanges and shielding these components from plasma contact. This narrower and deeper CHI gap will protect the vessel and PF-1C coil from excessive heat flux and protect the plasma from metal contamination, while continuing to provide the capability for CHI operations.

10.5.2.1. Divertor Cryo-pump

For boundary physics, a conceptual level design was performed on a closed divertor cryo-pump system as shown in Fig. 10.28(a) [8]. The initial indications are promising for providing divertor pumping for a relatively broad divertor parameter space including the snow-flake configuration. A physics design study of a cryo-pumping system for the NSTX-Upgrade has been performed; the results of the design were presented at the PAC-31 meeting and also at the APS-DPP meeting. A semi-analytic pumping model was used in this effort, and

extended to include the effect of finite plenum throat length on achievable neutral pressure. Recent NSTX experiments measuring the scaling of the divertor heat flux profile, as well as measurements of the electron temperature in the far SOL were used in this model to provide a semi-empirical projection of the pumping performance of candidate cryo-pumping geometries, as illustrated in Fig. 10.28 (b). This model was used to optimize the length, height, and radial position of the plenum entrance. Using the optimized entrance parameters, the achievable plasma density has been estimated by assuming a balance between neutral beam fueling and the pumped flux, and combining this with a two-point model for the SOL to relate the upstream and line-averaged density to the divertor density at which this balance is achieved. Pumping in the optimized configuration has been tested over a wide range of plasma position relative to the cryo-pump and flux expansion, and the modeling indicates that low plasma densities ($f_G \sim 0.5$) can be achieved over a broad range of configurations. Notably, the cryo-pump is found to be compatible with the high flux expansion Snowflake divertor, and in fact performs better in this configuration. Due to the improved power handling capability in this configuration, the allowable operating space with simultaneously sufficient pumping and low peak heat flux is larger with a Snowflake divertor. This work has been extended by using 2D plasma-neutrals modeling to evaluate pumping efficiency in radiative/detached regimes (which are not captured by the semi-analytic model used). The NSTX-U divertor cryo-pump engineering design will take place in FY 2014–15 and then component fabrication in FY 2016 and in-vessel installation in an extended outage in FY

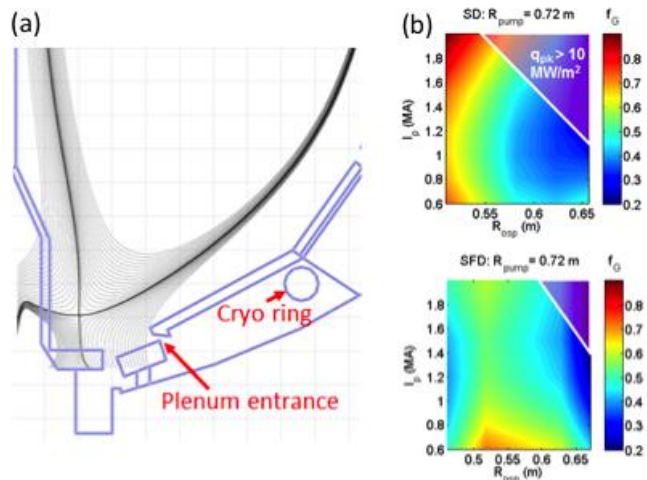


Fig. 10.28. (a) A conceptual design of divertor cryo-pump. (b) Projected density achievable for various R_{DSP} in standard and snowflake divertor configurations

2016 – 2017. The cryo-pump enables NSTX-U to establish density control without lithium coatings.

10.5.2.2. EHO antenna

Edge Harmonic Oscillations (EHOs) have been produced in lithiated NSTX discharges with the Mirnov amplitude of tenths of Gauss vs. ~ 3 Gauss for EHOs on DIII-D. External, adjustable control of edge density and pressure gradients enabled by the enhanced particle transport associated with EHOs of sufficient amplitude would be extremely valuable for NSTX-U, ITER and Demo. Initial calculations for NSTX-U indicate that EHOs may be efficiently driven with audio currents in HHFW antenna, using $\frac{1}{2}$ of the HHFW antenna driven by audio-amplifier system (which was built by PPPL for DIII-D) [9].

10.5.2.3. Fueling Tools

NSTX-U plasma operations will require the capability for gas injection from numerous locations. The gas injection systems on NSTX are not adequate to meet the physics program needs of NSTX-U as improvements are needed in the area of divertor heat flux mitigation, massive gas injection studies, and increased levels of gas injection from high-field side to meet the up to 10s discharge pulses planned for in NSTX-U. These are briefly summarized. Fig. 10.26 provides an overview of the different gas injection systems.

For normal inductive plasma operation, NSTX-U will rely on three mid-plane gas injectors as on NSTX. However, Injectors 2 and 3 are being relocated to bays I and G as their original location on Bay K is now taken up by the second neutral beam port. NSTX relied on two high-field side gas injectors. These were used for H-mode triggering, and the mid-plane injector was routinely used on most of the H-mode discharges. However, because of the short pulses in NSTX and narrow diameter pipe and long length, these could not be used in a controlled manner. These are being upgraded in NSTX-U to include large-diameter pipes so that the flow could be controlled and maintained during the 5-10s discharge pulses planned for in NSTX-U. In addition the system will have the capability for injection from two mid-plane locations and two locations from the region near the PF1A-U coil, as shown in Fig. 10.26. These will be toroidally displaced by 180 degrees. The higher flow-rates from these injectors may be required during Li conditioned operation on NSTX-U as the injectors on NSTX were at some times (such as during the diffusive Li coating experiments) were found to be inadequate to maintain the required electron densities in NSTX.

NSTX Upgrade Research Plan for 2014-2018

For CHI start-up, in addition to the existing gas injector on bay K bottom, a Tee will be added at Bay G bottom port, which is the location of lower divertor Penning gauge, and this too used to provide more control and improved toroidal gas injection symmetry.

HeGDC will use one of the mid-plane injectors as on NSTX. For boronization, the system is being significantly modified, by adding a new gas delivery system. In addition to the mid-plane injection, provisions will also be provided for gas injection from both the upper and lower divertor regions from the regions labeled as MGI in Figure 10.26. This is based on recent results from DIII-D that suggests that the divertor plates are much better conditioned with boron if the Tri-Methyl-Boron (TMB) that is included in the He carrier gas is injected from the divertor region.

For divertor heat flux mitigation studies, NSTX relied on a single gas injection location beneath the lower divertor plate on Bay-E. This capability will over a period of two years be expanded to two toroidal locations from the lower divertor and two toroidal locations from the upper divertor.

A supersonic gas injector (SGI) has been developed for fueling and diagnostic applications on NSTX. It is comprised of a graphite converging-diverging Laval nozzle and a commercial piezoelectric gas valve mounted on a movable probe at a low field side mid-plane port location. The SGI flow rate is up to 4×10^{21} particles/s, comparable to conventional NSTX gas injectors. The nozzle operates in a pulsed regime at room temperature and a reservoir gas pressure up to 0.33 MPa. The deuterium jet Mach number of about 4, and the divergence half-angle of $5^\circ - 25^\circ$ have been measured in laboratory experiments simulating NSTX environment. The SGI has been used for fueling of ohmic and 2-4 MW NBI heated L- and H-mode plasmas. Fueling efficiency in the range 0.1 - 0.3 has been obtained from the plasma electron inventory analysis. In NSTX, long-pulse discharge scenarios with controlled ion inventory have been demonstrated via the use SGI fueling and lithium-coatings for ion pumping. It is planned to continue using the SGI routinely in support of plasma operations on NSTX-U. In initial years, H-mode fueling scenarios with SGI fueling will be developed. A primary benefit of the SGI is a precise control of injected gas inventory. The SGI can support H-mode density limit and pedestal studies, as well as perturbative transport experiments. In later years, it is planned to integrate the SGI in a feedback-control loop for active density control with PCS. Another gas fueling method that is envisioned for NSTX-U is a cryogenic supersonic gas injection (also referred to as molecular beam injection). Recent fueling experiments at HL-2A and LTX indicated that molecular clusters obtained via cryogenic gas cooling could penetrate deeper into the plasma due to a much higher neutral density in a cluster jet and smaller ionization cross-sections of molecular clusters, thereby improving fueling efficiency of the supersonic gas injection even further.

10.5.2.4. Lithium Granule Injector for ELM Control

The lithium granular injector for ELM pacing [10] which was successfully demonstrated on EAST will be available for NSTX-U. The NSTX-U lithium granule injector (LGI) for ELM control has been completed in FY 2011 as shown in Fig. 10.29. The LGI system was shipped to the Chinese Academy of Science, institute of Plasma Physics and installed on the EAST Tokamak. The NSTX-U LGI system is capable of injecting horizontally redirected spherical Lithium granules (0.6 mm) at speeds approaching 100 m/s. The dropping rates (pacing frequencies) of 500 Hz have been achieved in the laboratory test.

A dropper apparatus allows the granule size to be changed between discharges. After an extended shake-down period, the injector was used to trigger/pace ELMs in EAST H-modes. Using Li granules with diameters of several tenths of a

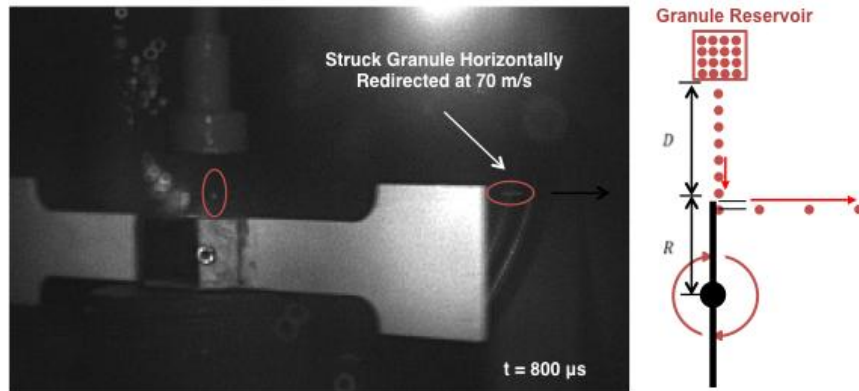


Fig. 10.29. NSTX-U lithium granular injector for ELM pacing.

millimeter injected at speeds of several tens of meters per second, ELMs were triggered at high efficiency. Pacing frequencies ranging between 10's to 100's of Hertz were observed. It is anticipated that much higher pacing frequencies can eventually be achieved using similar injector technology. The JET group is interested in the NSTX-U granular injector using beryllium granules for ELM pacing with application to ITER. A similar LGI system was also sent to RFX in Italy and successfully commissioned. An NSTX-U lithium dropper was also shipped to DIII-D for divertor recycling control.

10.5.2.5. Lithium Evaporator and Upgraded Lithium Coating Systems

With encouraging results in NSTX, the NSTX lithium evaporator (LITER) system as shown in Fig. 10.30(a) is planned for NSTX-U from Day 1 [11]. The LITER system is essentially a temperature controlled stainless steel container filled with liquid lithium (LL), with a nozzle to direct the lithium vapor for coating PFCs at desired locations.

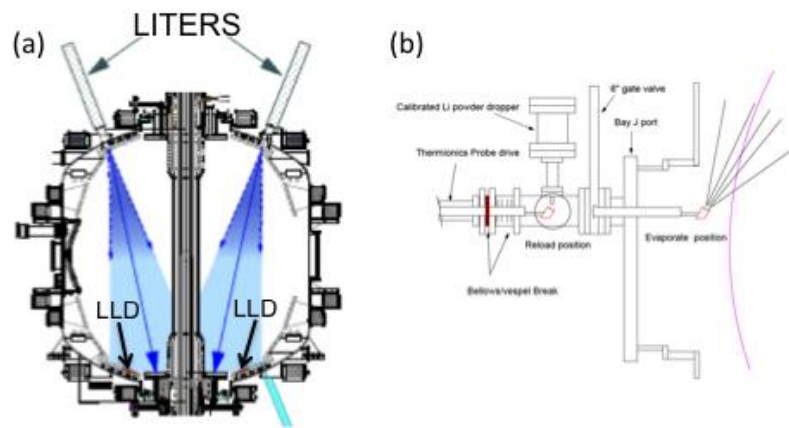


Fig. 10.30. (a) A schematic of the lithium evaporators (LITERS) injecting vapor which condenses on the room-temperature plasma facing components in the lower part of the vacuum chamber, including the lower divertor plates. (b) A schematic of the upward facing lithium evaporator concept.

The nozzle is typically aimed toward the middle of the inner divertor to maximize the lithium deposition on the divertor plates. Two LITERS units were used for better toroidal PFC coverage of lithium on NSTX. The units each have a 90 g lithium capacity. The LITER consists of a main reservoir oven and an output duct to allow insertion in a PFC gap in the upper divertor region. Two heaters were used on each LITER, one heater on the output duct and one heater on the main reservoir. The heater on the main reservoir was typically operated to maintain the LL temperatures of 600–650 °C which enables an adequate lithium evaporation rate, as this rate increases rapidly with temperature. The heater on the output duct was operated about 50–100 °C hotter than the heater on the main reservoir to reduce lithium condensation on the output duct aperture. Typical evaporation rates have been in the range of 1 to 40 mg/min. The lithium evaporation typically takes place between plasma discharges to obtain the desired level of lithium coating on the PFCs, which could be in the range of 30 – 500 nm thick. In NSTX, nearly 1,000 g of lithium was delivered onto the PFCs during the last experimental campaign in FY 2010-2011. For the initial NSTX-U lithium capability, the baseline is the dual upper and lower aiming evaporators and a new Li granular injector on the mid-plane. A design is being developed for an upper aiming evaporator to cover the upper divertor region. An example of a possible system is shown in Fig. 10.30 (b). The mini Li evaporator concept requires a lithium dropper as a source to fill a Li crucible which is then inserted into the edge of NSTX-U well outboard of the SOL, and heated to above 700 °C to cause rapid evaporation of the Li powder. Electron beam heating is the leading candidate for a heat source. Due to the high temperature, all Li is promptly evaporated to the upper vessel. This has advantages of requiring no shutters after evaporation. Since the

evaporator is outside of the plasma volume, the discharge can commence without retracting the evaporator. This reduces the time between the end of the evaporation and the start of the discharge ensuring minimal passivation of the fresh lithium.

10.5.2.6. High-Z Metallic Divertor

While the baseline NSTX-U operation plan is to start with all graphite tiles, in view of the natural progression toward future facilities such as FNSF, it is important to investigate the viability

of high-Z metallic divertor on NSTX-U. After making an assessment of all graphite PFC plasma operations, a row of high-Z tiles will be installed on lower OBD (outboard divertor) region as shown in Fig. 10.31. By placing the high-Z divertor PFC at larger major radius on

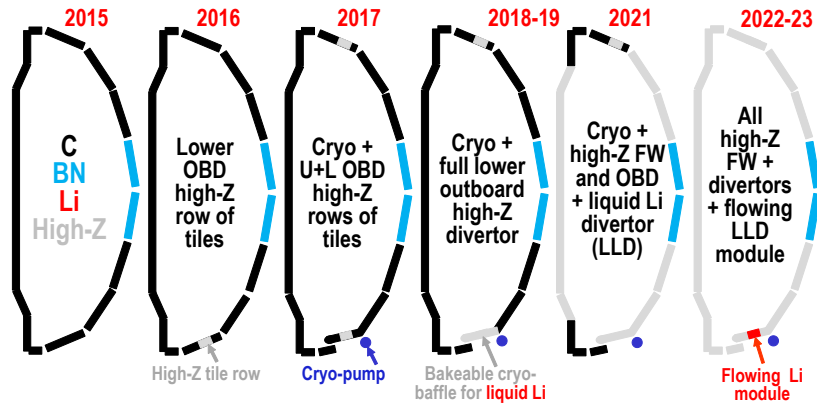


Fig. 10.31. Nominal implementation plan of boundary physics capability including cryo-pump and high-Z PFCs + Liquid Li Divertor module with 5 YP base funding.

the OBD, the risk to standard high-delta shapes and scenarios is minimized as was the case for the original LLD. The high-Z tile design will be assessed for tolerance to thermal and disruption loads. This plan enables a transition to high-Z PFCs to support PMI/FNSF next-steps. With the OBD high-Z tiles, erosion and migration of high-Z tile materials to be transported into the plasma core can be investigated with and without lithium. Additional high-Z tiles will be installed in conjunction with the installation of the cryo-pump in FY 2016 – 17 long outage. It is envisioned that both upper and lower divertor surfaces will be covered by high-Z material by 2018.

10.5.2.7. High-Z Outer and Inner Wall PFCs

As noted above in Section 10.5.2.6, the present NSTX-U PFC strategy is to start with all graphite tiles for Day 1 and progress in stages with rows of high-Z tiles as shown in Fig. 10.31. After assessing the plasma behavior and the high-Z tile performance, the entire NSTX-U PFC will be replaced with high-Z PFCs. One can envision TZM or W (tungsten) lamellae or tiles if workable. For low heat flux regions such as the passive plates and CS off-midplane, one may use W-coated graphite tiles.

10.5.2.8. Flowing Liquid Lithium Divertor/Module

Various concepts are being considered for a liquid lithium divertor system [12]. A flowing liquid lithium loop R&D facility (LDRD funded) is being built at PPPL [Fig. 10.32]. If successful, the design will be adapted for NSTX-U. The HT-7 tokamak is also testing liquid lithium PFCs. Development of flowing liquid lithium PFCs and related technologies is also underway at PPPL supported by the LDRD funding which if successful could be adopted as the NSTX-U liquid lithium divertor. The present efforts focus on a capillary-restrained system that incorporates gaseous cooling. In this conceptual diagram, “T-tubes” are considered for the active cooling scheme with either helium or super critical-CO₂ (s-CO₂) as the primary coolant. The PFC includes a porous or textured front face, similar to that used on LLD for liquid lithium stability against disruptive loads. Lithium flow channels are located parallel to the cooling channels with discrete ports to allow the liquid metal to wick quickly to the front-face. In addition to size scaling, an examination of the basic cooling fluid is also being carried out. S-CO₂ has been identified by many in the fission power industry as having favorable properties in a power cycle over helium. Experimental demonstration of liquid metal PFC concepts is currently underway to complement the design studies described above. These begin with the development of a liquid lithium loop which will provide active pumping into and out of

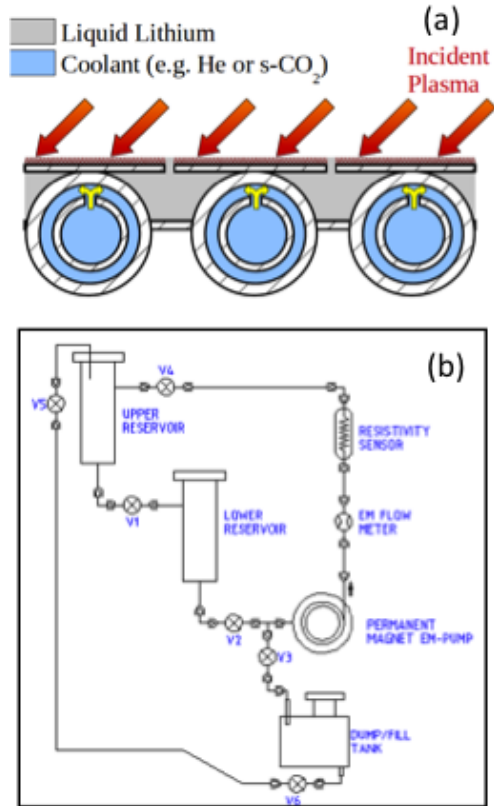


Fig. 10.32. Liquid lithium R&D. (a) A conceptual capillary-based lithium divertor PFC design. (b) A flowing liquid lithium test loop.

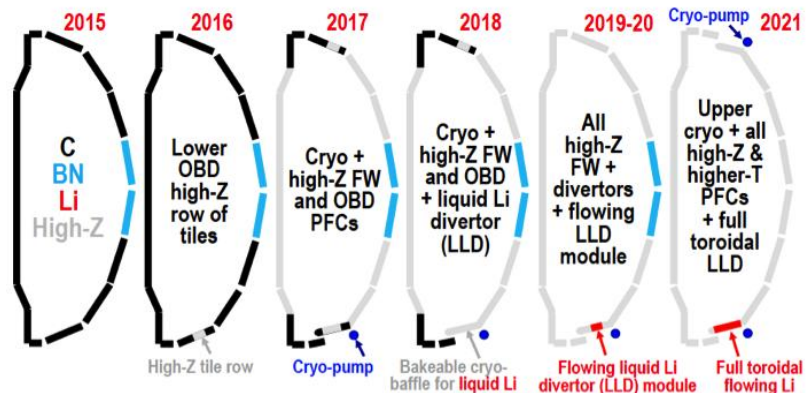


Fig. 10.33. Nominal implementation plan of boundary physics capability including cryo-pump and high-Z PFCs + Liquid Li Divertor module with 5 YP incremental funding.

These begin with the development of a liquid lithium loop which will provide active pumping into and out of

vacuum chambers. The facility will be utilized for testing of candidate PFC designs to show such things as (1) stable operation and flow in a tokamak-relevant vacuum environment (10^{-7} to 10^{-6} Torr pressures), (2) restart capability after periodic shut-down and gettering of residual gases, (3) maintainability and reliability in addition to safe operation. Future plans include active purification of lithium inventory and upgrades to include integrated tests with s-CO₂ cooling systems. The boundary physics capability plan would be modified with the incremental funding as shown in Fig. 10.33.

10.5.2.9. Laboratories for Material Characterization and Surface Chemistry

NSTX-U is collaborating with two new laboratories established at PPPL in collaboration with Princeton University dedicated for materials characterization and surface chemistry experiments. The Surface Science and Technology Laboratory is equipped with three surface analysis systems and an ultrahigh vacuum deposition chamber. Substrates for vapor deposition of metal films can be heated and cooled from 85 – 1500K using liquid nitrogen cooling and resistive and electron-beam heating. These systems have a variety of surface diagnostics, including high resolution electron energy loss spectroscopy (HREELS), which is capable of probing both optical and vibrational excitations over a wide range of 0 - 100 eV with an electron energy resolution of 3 meV, alkali ion-scattering spectroscopy (ALISS), and angle-resolved X-ray photoelectron spectroscopy (XPS). Another instrument has XPS, low energy ion scattering (LEIS), and reflection high-energy electron diffraction (RHEED) capability for thin film growth studies. In this laboratory, the time evolution of the chemical composition of lithium surfaces exposed to typical residual gases found in tokamaks was recently measured. Solid lithium samples and a TZM alloy substrate coated with lithium have been examined using XPS, temperature programmed desorption (TPD), and Auger electron spectroscopy (AES) both in ultrahigh vacuum conditions and after exposure to trace gases. Lithium surfaces near room temperature were oxidized after exposure to 1-2 Langmuirs ($1\text{L}=1\times 10^{-6}$ torr s) of oxygen or water vapor. The oxidation rate by carbon monoxide was four times less. An important result of the measurements for NSTX-U is that lithiated PFC surfaces in tokamaks were found to be oxidized in about 100 s depending on the tokamak vacuum conditions which is much less than a typical time duration between the tokamak plasma shots [12]. A second laboratory, the Surface Imaging and Microanalysis Laboratory, contains a high-performance field emission Auger and multi-technique surface microanalysis instrument with a field emission electron source and lateral resolution of 30 nm for elemental analysis of surfaces of samples on the micro and nano scale.

10.5.3. Start-up and Ramp-up

10.5.3.1. CHI upgrades

A significant new upgrade for CHI is the improved location of both the injector and absorber buffer field coils [13]. In a CHI discharge the maximum plasma current CHI can generate is directly proportional to the magnitude of the injector flux. As shown in Fig. 10.34, the injector coil on NSTX-U is positioned much closer to the CHI gap. This allows more of the flux generated by this coil to connect the inner and outer divertor plates. This increases the theoretical injector flux capability in NSTX-U to over 300 mWb, compared to a maximum of 80 mWb in NSTX. To put this in perspective, a low inductance 1 MA discharge in NSTX-U will contain on the order of 200 to 250 mWb of poloidal flux. To control a condition known as absorber arcs, NSTX relied on two small coils located on top of the machine that were dedicated to providing a buffer field to keep the expanding CHI discharge from contacting the upper divertor plates and generating an absorber arc. On NSTX-U these dedicated coils are not necessary as the main PF1C-U coil that is located closer to the absorber gap more than doubles the current capability and the current slew rates of the absorber buffer field coils used on NSTX. The key parameters for the CHI system for NSTX and NSTX-U are given in Table 10.1.

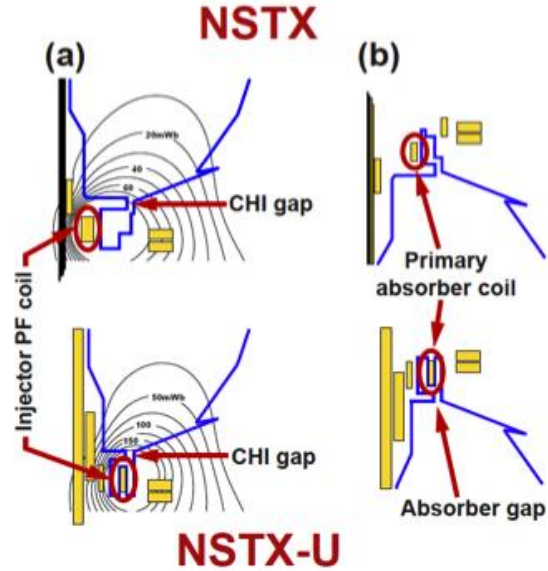


Fig. 34. A schematic of old and new CHI system configuration.

Parameters	NSTX	NSTX-U
R(m)	0.86	0.93
a(m)	0.68	0.62
B ₀ (T)	0.55	1.0
Toroidal Flux (Wb)	2.68	3.78
Normalized internal inductance, \bar{l}_i	0.35	0.35
Full non-inductive sustainment current, Max I _p (MA)	0.7	1
Poloidal Flux for Max I _p (mWb)	132	206
Required Injector Flux for 50% Max I _p (mWb)	66	103
Current Multiplication factor	41	37
Peak current multiplication	53	48
Peak startup current (kA)	450	650
Injector current	8.6	13.6
Maximum available Injector Flux (mWb)	63-80	220-340
Max startup current potential (kA)	~400	~1 MA
Required injector current For Max current potential (kA)	10	27*

Table 10.1. Comparison of the NSTX and NSTX-U CHI system parameters

10.5.3.2. Plasma Gun Start-Up

The conceptual design for the NSTX-U compact helicity injection startup system is presently under development by the University of Wisconsin PEGASUS group [14].

Figure 10.35 shows a top-down view of the proposed injector, with explicit detail of the gate valve, injector “garage”, bellows structure, and the umbilical cables and tubing. Machine access would be through a large (8-inch diameter or larger) off-midplane port on the outboard side. The injector is shown inserted between two passive plates, though those details are dependent on the exact port that is made available on NSTX-U for these studies. A more detailed insert shows the elements of the pre-conceptual injector, including the limiter, the arc tube surrounded by an electrode, and an insulating surface behind the electrode to prevent arcing back along the field lines.

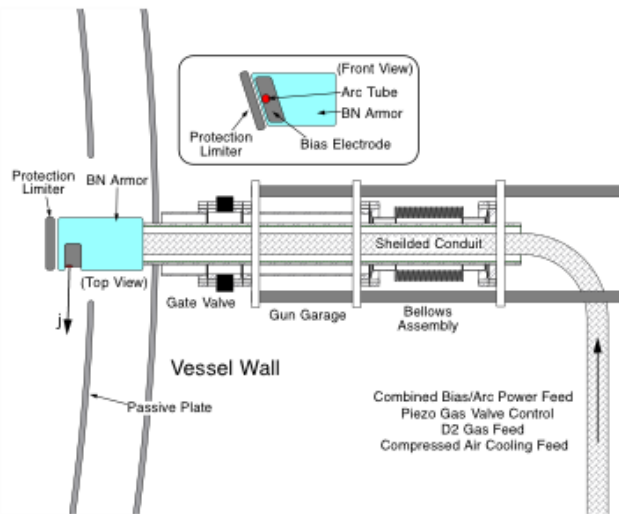


Fig.10.35. Detailed view of pre-conceptual PEGASUS point-source helicity injector gun design.

The present design uses boron nitride as both the insulating surface and the plasma-facing armor for the sides of the injector. The final conceptual design may well use molybdenum or tungsten armor around and behind the injector, in order to shield the boron nitride from plasma impact. The injector will be designed to be fully retractable, using a bellows drive for vacuum integrity, and will be kept outside the NSTX-U vessel and behind a gate valve (in a “garage” region) when not in use. The plasma-facing portion of the injector will incorporate a limiter structure, an active plasma gun (the arc tube), and a passive electrode. The electrode will be shaped, as much as possible within the footprint of the port, to maximize the Taylor limit while keeping an adequate cross-section for the corresponding current drive. The umbilical cables, tubing, and diagnostic lines from the injector to the power supplies and control system will be kept in a shielded conduit, both to isolate the diagnostic lines from external noise sources and to mitigate the electrostatic noise associated with high-power switching of the injector H-bridge bias supply. Deuterium gas for the active plasma gun is supplied through flexible tubing, with most fueling during the electrode-drive phase supplied through the usual NSTX-U fueling valves. The power supplies and control system can be relatively compact, depending upon the total stored energy that will be necessary for driving the bias during the high-current startup scenario. A simple pulse-forming network will provide the arc

discharge in the active plasma source, with a crowbar switch on the outputs to the arc tube. The bias power supply will be based on the technology used on the Pegasus Toroidal Experiment, with an array of reduced H-bridge supplies providing the required current and voltage. The arc supply, bias bridges, deuterium gas supply, and control systems will perhaps occupy the volume of an office desk. The total stored energy for the bias supply, necessary for a high-current startup scenario, remains to be determined.

10.6 NSTX-U Diagnostic System Status and Plans

The NSTX-U diagnostic planning meeting was held in July 2011 and also in July 2012. Since the 2012-2016 non-laboratory NSTX-U diagnostic grant recipients were decided in FY 2012, they represent a significant fraction of the planned NSTX-U diagnostic capability. The diagnostics which were operational in FY 2011 are generally expected to be available for the NSTX-U operation unless otherwise noted. A list of the existing diagnostic systems which are expected to be available for NSTX-U within two years of operation is shown in the Table 10.2. We note that at least half of those diagnostic systems have strong collaboration components. We shall describe major diagnostic systems in the following sections.

<p>MHD/Magnetics/Reconstruction Magnetics for equilibrium reconstruction Halo current detectors High-n and high-frequency Mirnov arrays Locked-mode detectors RWM sensors (n = 1, 2, and 3)</p> <p>Profile Diagnostics MPTS (42 ch, 60 Hz) T-CHERS: $T_i(R)$, $V_\phi(r)$, $n_c(R)$, $n_{Li}(R)$, (51 ch) P-CHERS: $V_\theta(r)$ (71 ch) MSE-CIF (18 ch) MSE-LIF (20 ch) Midplane tangential bolometer array (16 ch)</p> <p>Turbulence/Modes Diagnostics Tangential microwave high-k scattering Beam Emission Spectroscopy (48 ch) Microwave Reflectometer, Microwave Polarimeter Ultra-soft x-ray arrays – multi-color</p> <p>Energetic Particle Diagnostics Fast Ion D_α profile measurement (perp + tang) Solid-State neutral particle analyzer Fast lost-ion probe (energy/pitch angle resolving) Neutron measurements Neutral particle analyzer</p>	<p>Edge Divertor Physics Gas-puff Imaging (500kHz) Langmuir probe array Edge Rotation Diagnostics (T_i, V_ϕ, V_{pol}) 1-D CCD H_α cameras (divertor, midplane) 2-D divertor fast visible camera Metal foil divertor bolometer AXUV-based Divertor Bolometer IR cameras (30Hz) (3) Fast IR camera (two color) Tile temperature thermocouple array Divertor fast eroding thermocouple Dust detector Edge Deposition Monitors Scrape-off layer reflectometer Edge neutral pressure gauges Material Analysis and Particle Probe Divertor Imaging Spectrometer</p> <p>Plasma Monitoring FReTIP interferometer Fast visible cameras Visible bremsstrahlung radiometer Visible and UV survey spectrometers VUV transmission grating spectrometer Visible filterscopes (hydrogen & impurity lines) Wall coupon analysis</p>
--	---

Table 10.2. Existing NSTX-U Diagnostic Systems

10.6.1. Profile Diagnostics

10.6.1.1. Multi-Pulse Thomson Scattering System

Twelve additional channels bringing the total number of channels to 42 for the multi-pulse Thomson scattering (MPTS) system were installed and commissioned in FY2011. After acceptance testing, the new polychromators were first assembled and aligned, and then installed in the MPTS room. The optical fiber bundles bringing scattered light from the plasma were then reconfigured to produce the desired spatial distribution of measurement points. The locations of all the MPTS

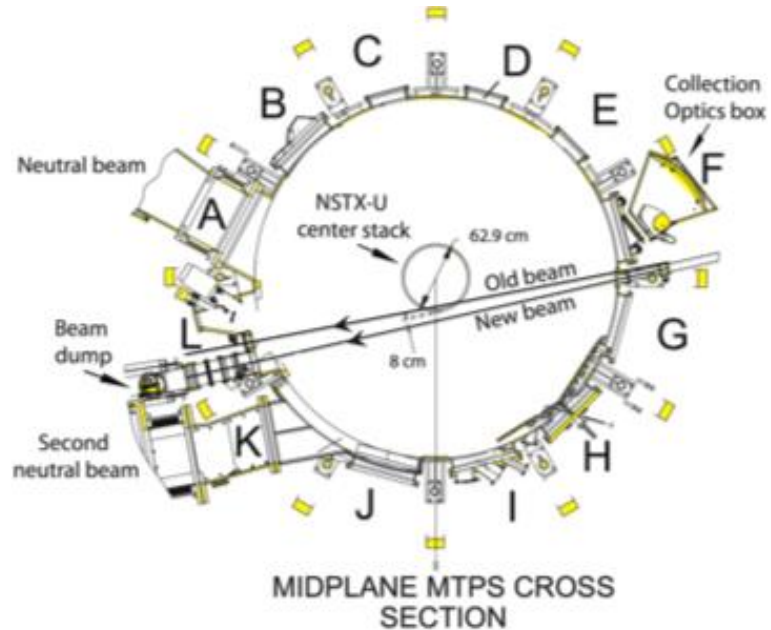


Fig. 10.36. Mid-plane cross section of NSTX-U showing old and new MPTS laser beam paths, relocated laser input port on the vacuum vessel, new beam dump, and scattered light collection optics box.

channels were then measured by back-illumination along each fiber of a target plate mounted inside the vacuum vessel. The spectral transmission curve of each polychromator was then measured with a scanning monochromator and the overall calibration was performed *in situ* by employing Rayleigh and Raman scattering of the light from the MPTS laser system by nitrogen and argon introduced into the vacuum vessel. Measurements of the optical transmission of the observation window were also made to establish a baseline for monitoring its evolution through the run. The upgraded MPTS system with 42 total channels was ready for operation in July 2011.

Modifications to the Multi-Pulse Thomson Scattering (MPTS) diagnostic required for the NSTX Upgrade were designed, and fabrication and procurement of the needed components were started [15]. The larger diameter of the center stack in NSTX-U requires that the MPTS laser beams be re-aimed to avoid striking the center stack, which would cause damage to it as well as an unacceptable level of scattered laser light in the vacuum vessel [Fig. 10.36]. The re-aiming of the laser beams requires several other changes to the MPTS diagnostic configuration: 1) a new laser beam dump must be provided on a new vacuum vessel port structure on the opposite side of the vacuum

vessel (Bay L) from the laser input port; 2) the laser input port on the vacuum vessel must be moved several centimeters on the vacuum vessel and re-aimed to achieve the needed laser beam path; and 3) the MPTS light collection optics must be modified and re-aimed to provide high-resolution imaging of the re-aimed laser beam. This new configuration is shown in Figure DIAG-1. Redesigning the MPTS system to meet these requirements was accomplished and a successful preliminary design review was held. A successful final design review for the modifications to the vacuum vessel was held, and final design reviews for the remaining modifications to the system are planned for early FY2013. The new port structure required for the laser beam dump is located at Bay L and includes ports for several other diagnostics. The reconfigured MPTS diagnostic will be installed prior to NSTX-U first plasma and commissioned in early experimental operation following first plasma.

10.6.1.2. Charge-Exchange Recombination Spectroscopy

10.6.1.2.1. Toroidal and Poloidal CHERS

The NSTX-U charge exchange recombination spectroscopy (CHERS) diagnostic suite measures impurity ion temperature, impurity flow, and impurity density [16]. A schematic of the system is shown in Fig. 10.37. Together, these measurements can be used to determine the radial electric field in the plasma. The CHERS systemsⁱ on NSTX-U use the $n = 8-7$ transition of the C^{5+} ion at 529.1 nm to infer the temperature, density, and velocity of the parent ion C^{6+} . Along with the charge exchange emission, intrinsic background emission from C^{5+} ions is also present. Dedicated views that do not intersect the beam are used to measure this background emission. Both

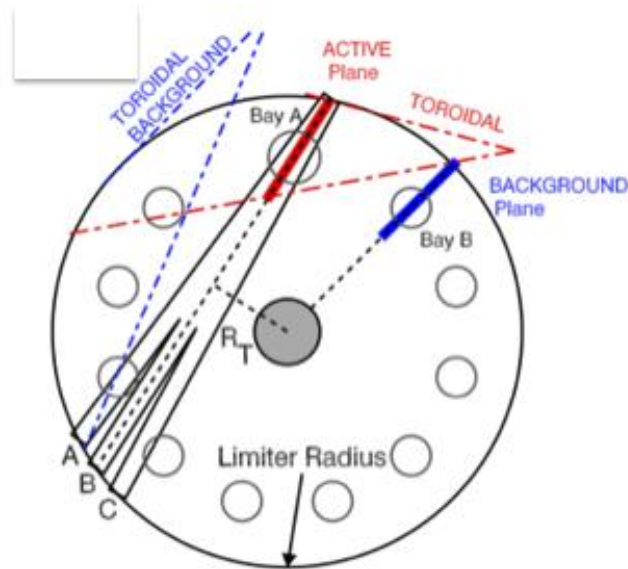


Fig. 10.37. Plan view of NSTX-U midplane showing the locations of the active and background detection planes for the poloidal CHERS views. The active plane shares the same tangency radius (R_T) as the central beam. Also shown are the range of the toroidal CHERS views and the corresponding background views.

poloidal and toroidal viewing CHERS systems are used on NSTX. An absolute photometric calibration is performed allowing accurate carbon density profile measurements. Profile measurements are obtained every 10 ms.

The toroidal viewing system is situated at the plasma midplane. Two sets of sightlines view across the neutral beams and parallel to the neutral beams to provide active measurements and simultaneous independent background measurements. The active view has 51 spatial channels across the midplane, while the background view consists of 39 spatial channels. The radial resolution is variable, about $\Delta r = 0.6$ cm near the edge and increasing to about $\Delta r = 3.0$ cm in the core. With the low magnetic field typical of the spherical torus, the edge resolution is comparable to the gyro radius. The toroidal viewing optics are shared with the Motional Stark Effect (MSE) diagnostic.

The poloidal viewing CHERS has matched symmetric views from above and below the plasma. The upper and lower sightlines are precisely aligned where they intersect at the midplane. The active plane of measurement is aligned with the central neutral beam trajectory. The background emission is measured in a radial plane at a toroidal location about 30° from the neutral beams. Higher resolution is provided in the outer portion of the plasma ($R \geq 120$ cm) with twice as many sightlines. The poloidal viewing system is sufficient to measure line-integrated velocity. To obtain local poloidal measurements, an inversion is performed, which requires information from the toroidal viewing system. The radial resolution after inversion is $\Delta r = 0.6$ cm in the outer range and $\Delta r \leq 1.8$ cm near the plasma center, comparable to the toroidal viewing system.

The NSTX Upgrade introduces an additional set of neutral beam sources (NB2) with larger tangency radii than the original set of neutral beams (NB1). NB2 sources are in the field of view of the CHERS background sightlines, preventing the independent measurement of background emission when they are operated. When only the original neutral beam sources (NB1) are used, the existing analysis techniques can still be used. When any of the new neutral beam sources (NB2) are used, another method must be used for analysis. One possibility is to modulate a neutral beam to provide the background measurement, either NB1 or NB2. However, there may be limitations to the number of modulations allowed during a discharge. The quality and time resolution of the CHERS measurements will be degraded with the operation of the NB2 sources.

10.6.1.2.2. Edge Rotation Diagnostic

This collecting lens for the CHERS background is shared by the toroidal views of an edge Doppler spectrometer (ERD), which measures emission from C^{2+} , He^+ , Li , and

Li^+ [18]. The collecting lens for the background poloidal CHERS views at the top of NSTX-U is shared by the ERD system providing poloidal velocity measurements. Seven toroidal channels and six poloidal channels are used. The spatial resolution of the ERD is ~ 3 cm with a time resolution of 10 ms. The radial electric field near the edge can be computed using the toroidal and poloidal velocity measurements of C^{2+} or He^+ . During HHFW operation, the ERD is used to monitor the anisotropic ion heating near the plasma edge.

10.6.1.3. Soft X-ray Diagnostics

A suite of new and upgraded soft X-ray (SXR) to VUV diagnostics based on the multi-energy imaging technique developed in the previous NSTX research will be installed on NSTX-U by the Johns Hopkins group [18-19]. The SXR-VUV diagnostic suite will enable improved measurements of the impurity content and radial transport, of radial and toroidal MHD mode structure and of Te profiles and perturbations in the core, edge and divertor, and in all NSTX-U operating scenarios, from non-inductive start-up and sustainment, to high power beam and RF driven regimes. A layout for the in-vessel, atmospheric re-entrant EDGE and CORE ME (multi-energy)-SXR system, as well as the fast (100Hz) Transmission Grating Imaging Spectrometer is shown in Fig. 10.38.

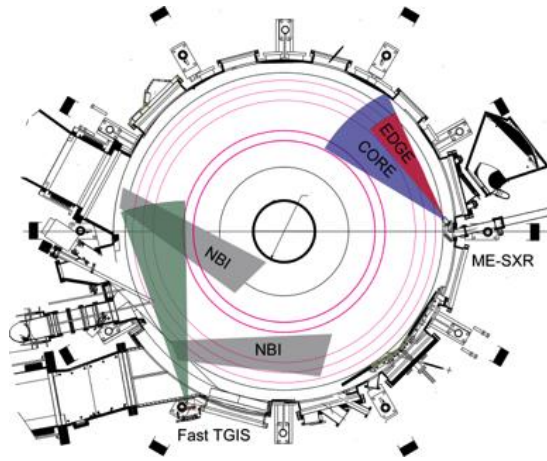


Figure 10.38. Plan view for the in-vessel, atmospheric re-entrant EDGE and CORE ME-SXR system, as well as the fast (100Hz) Transmission Grating Imaging Spectrometer

A system of two toroidally displaced, edge and core in-vessel tangential ME-SXR arrays. This system will simultaneously measure the core and edge plasma emission profiles in up to five energy bands spanning the range from a few eV (bolometry) to several keV, and at two toroidal locations separated by $\sim 90^\circ$. Each of the two toroidally displaced tangential arrays will include an edge sub-array covering the region $0.6 < r/a < 1$ with 1 cm resolution and a core sub-array covering the entire inboard to outboard plasma with ≥ 3 cm resolution. The time resolution will be $\geq 10 \mu\text{s}$. The high spatial resolution combined with energy resolution and extended toroidal coverage will enable the following multiple physics capabilities:

- Impurity and electron thermal perturbative transport measurements from the edge to the core using gas puffs and the repetitive laser blow-off proposed below,

NSTX Upgrade Research Plan for 2014-2018

- Fast, high resolution measurements of edge Te profiles (and with external ne constraint also n-z profiles) for ELM studies, for edge code validation, and for improved edge stability analysis,
- Fast, toroidally resolved measurements of edge and core Te, n-z profiles and perturbations for the study of 3D-field effects, RWMs, and disruptions,
- Real-time Te and Zeff measurements for stability prediction and feedback control development, and
- Enhanced sensitivity non-magnetic toroidal mode identification for disruption sensing.

The ME-SXR array diagnostic has been successfully prototyped and tested in our recent NSTX research. For NSTX-U we will develop an *in-vessel* design that will enable implementing the arrays without requiring mid-plane port space, which will be scarce on NSTX-U due the addition of the second neutral beam.

A fast tangential Transmission Grating Imaging Spectrometer (TGIS) This device is an upgrade of the TGIS diagnostic implemented on NSTX and will enable absolute impurity spectra measurements in the XUV range (50-800 Å) with high time resolution (≥ 5 -10 ms) and with high space resolution (≥ 2 cm). The instrument will have a tangential view of a heating beam, enabling simultaneous diagnostic of low-Z impurities through the beam excited CX emission and of the high-Z impurities through the combined electron and beam excited emission. The upgraded TGIS will enable routine measurements of the radial profile of all impurity fractions in NSTX, from lithium to molybdenum, for an accurate modeling of the ME-SXR profiles from the edge to the core and for an improved impurity monitoring capability in all NSTX-U operating scenarios, including noninductive startup and sustainment.

A repetitive laser blow-off system for multiple injections of non-recycling impurities during the shot - A laser blow-off (LBO) system, which will ablate a thin film of material from a glass slide, injecting a short burst of neutral impurity atoms into NSTX-U plasmas for impurity and electron thermal perturbative transport measurements, will be implemented by the JHU group. A high-powered Nd:YAG 1064 nm laser, with pulse energy ≥ 800 mJ and pulse frequency ≥ 10 Hz, will be utilized. It should be also noted that the same laser and optical configuration, with the addition of in-vessel steerable optics, can be used for laser-induced breakdown spectroscopy (LIBS) of in-vessel PFC components as proposed by Purdue University which would allow in-situ, real-time characterizations of surface impurities, concentrations, and erosion/deposition rates between discharges in NSTX-U

10.6.1.4. Motional Stark Effect – Collisional Induced Fluorescence

With a doubling of the magnetic field as part of the NSTX upgrade the Motional Stark Effect measurement based on Collisionally Induced Fluorescence (MSE-CIF) collection optics can be optimized to increase the throughput [20]. A schematic of the MSE-CIF system is shown in Fig. 10.39. An aperture on the collection optics is used to reduce the geometric broadening. With the higher field this will change the optimal aperture width and polarization fraction for maximizing the signal-to-noise. We will use our numerical models and optical design code to re-optimize the aperture width. To support its Five Year Plan, the NSTX-U team has expressed a desire for more flexibility from the MSE measurement. The neutral beams will only be able to inject for three seconds at 90 kV, or five seconds 80 kV. With the possibility of long NSTX-U discharges, it would be desirable if MSE can switch from viewing one neutral beam to another within a single discharge to provide data over long pulse discharges. Preliminary tests have shown that this can be accomplished with the existing high voltage power supplies on the birefringent filters. We propose adding a high voltage relay bridge that will provide fast tuning during a discharge. The bridge circuit will allow switching both the voltage amplitude and polarity. This will enable the MSE-CIF system to switch between beams with a time delay of less than 200 ms. The MSE-CIF system will start with 18 sightlines but the real-time capability will be also implemented as described in (10.6.3.2). The MSE-CIF system is upgradable to 40 sightlines budget permitting.

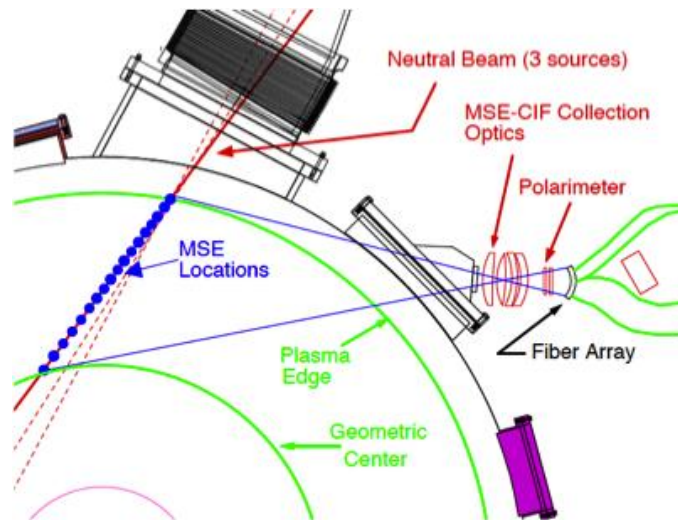


Figure 10.39. MSE-CIF layout on NSTX-U with radial locations indicated by the blue dots along the neutral beam trajectory.

The neutral beams will only be able to inject for three seconds at 90 kV, or five seconds 80 kV. With the possibility of long NSTX-U discharges, it would be desirable if MSE can switch from viewing one neutral beam to another within a single discharge to provide data over long pulse discharges. Preliminary tests have shown that this can be accomplished with the existing high voltage power supplies on the birefringent filters. We propose adding a high voltage relay bridge that will provide fast tuning during a discharge. The bridge circuit will allow switching both the voltage amplitude and polarity. This will enable the MSE-CIF system to switch between beams with a time delay of less than 200 ms. The MSE-CIF system will start with 18 sightlines but the real-time capability will be also implemented as described in (10.6.3.2). The MSE-CIF system is upgradable to 40 sightlines budget permitting.

10.6.1.5. Motional Stark Effect – Laser Induced Fluorescence

The Motional Stark Effect measurement based on Laser Induced Fluorescence (MSE-LIF) diagnostic as shown in Fig. 10. 40 will provide measurements of the field line pitch angle profile without requiring injection of the heating neutral beam needed for the present MSE system on NSTX-U which is based on collisionally induced fluorescence (MSE-CIF) [21]. It will therefore provide critical data for measuring RF-driven current in NSTX-U without the competing effect of current driven by the heating neutral beam. Also, direct reconstruction of the total plasma pressure profile should be possible from its

capability to make local measurements of the total magnetic field in the plasma. Combining this measurement with the comprehensive thermal profile measurements

already available on NSTX-U, the fast-ion pressure profile can be inferred and compared to prediction to determine the influence of Alfvén Eigenmodes and other MHD activity on fast-ion confinement. Furthermore, the data from the two MSE systems,

MSE-CIF and MSE-LIF, can be combined to calculate the radial electric field profile, an important element in plasma transport research. In collaboration with researchers from Nova Photonics Inc., the installation and commissioning of the first three channels of the Motional Stark Effect measurement based on Laser Induced Fluorescence (MSE-LIF) was completed in August 2011. After extensive development and testing in the laboratory, the diagnostic neutral beam, surrounded by a two-layer magnetic shield, was mounted on its stand and connected to the NSTX-U vacuum vessel, its power supplies and other services. After commissioning its control and interlock systems operation of the diagnostic neutral beam was achieved. The development of a high-power, narrow-line laser source for excitation of the injected neutrals was completed and the laser was installed. The viewing optics, filters and detectors for 10 sightlines crossing the neutral beam path were designed, procured and installed. Finally, in September, the magnetic field sensitivity of the MSE-LIF system was tested by injecting the neutral beam into deuterium gas introduced into the NSTX-U vacuum vessel with up to 3mT applied by the poloidal field coils. In this test, the MSE-LIF system was able to distinguish changes of less than 1mT. For NSTX-U Day-1 operation, 20 sightlines of the MSE-LIF system will be available.

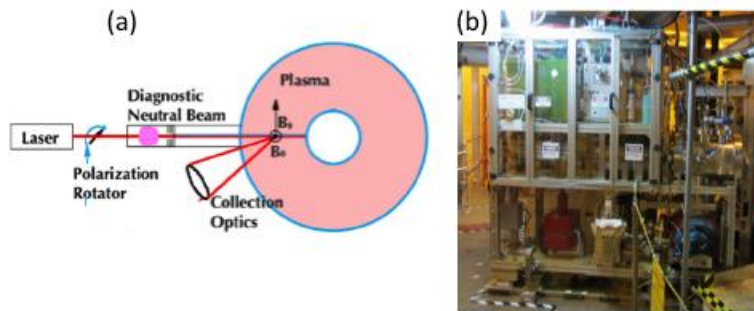


Fig. 10.40. MSE-LIF System: (a) NSTX MSE-LIF system layout schematic, (b)MSE-LIF system installed on NSTX.

10.6.2. Turbulence Diagnostics

For turbulence diagnostics systems, the high-k scattering system detector array presently located at Bay K will have to be relocated to Bay L after the 2nd NBI installation at Bay K [22]. By re-aiming the microwave beam, it is possible to measure both the radial and poloidal components of the high-k turbulence. The existing 280 GHz system will be replaced by a ~600 GHz system. The higher frequency system is designed to improve high-k resolution and SNR. For low-k turbulence, the beam emission spectroscopy (BES) system with a new generation of BES detector has been developed by the University of Wisconsin group. The group is planning to expand the BES system from

28 spatial channels to 48 channels for NSTX-U. A 288 GHz polarimetry system for magnetic fluctuation measurements is presently being tested on DIII-D. For the edge region, the gas puff imaging (GPI) diagnostic will be implemented.

10.6.2.1. High-k Scattering System

The 280 GHz high-k tangential scattering system of NSTX will be replaced by a 604 GHz poloidal scattering system being developed by UC Davis for NSTX-U, thereby considerably enhancing planned turbulence physics studies by providing a measurement of the k_θ -spectrum of both ETG

and ITG modes. The probe beam in this case will enter the plasma from a port on Bay G while a tall exit window located on Bay L will be employed to collect the poloidally-scattered beams and image them onto an array of 5-8 waveguide mixers. The reduced wavelength in the poloidal system will result in less refraction and extend the poloidal wavenumber coverage from the current 7 cm^{-1} up to $> 40 \text{ cm}^{-1}$. As pointed out earlier, measuring the k - θ spectrum as well as k - r spectrum is crucial for identifying the source of turbulence since the 2D k -spectra driven by different instabilities have different anisotropies. More importantly, the peak of the 2D k -spectrum has to be measured so that the turbulence amplitude can be experimentally correlated to observed plasma transport. The unique property of this new high-k scattering system is that it uses only one microwave launching system but is able to achieve four scattering configurations, which are sensitive to different regions of the turbulence 2D k -spectrum owing to the large magnetic shear in NSTX-U. The probe beam and two scattering beams for the two toroidal scattering schemes are plotted in Fig. 10.41 (a); here the probe beams are tilted toroidally with respect to the scattered beams for +’ve and -’ve radial scattering. In the poloidal scattering arrangement of Fig. 10.41 (b), the first scheme, plotted in blue, has scattered beams going upward in the positive Z direction (upward scattering) while the other scheme, plotted in red, has scattered beams going downward in the negative Z direction (downward scattering). A total of four scattering schemes is thus possible with different combinations of toroidal and poloidal tilt angles. It is noted that the proposed

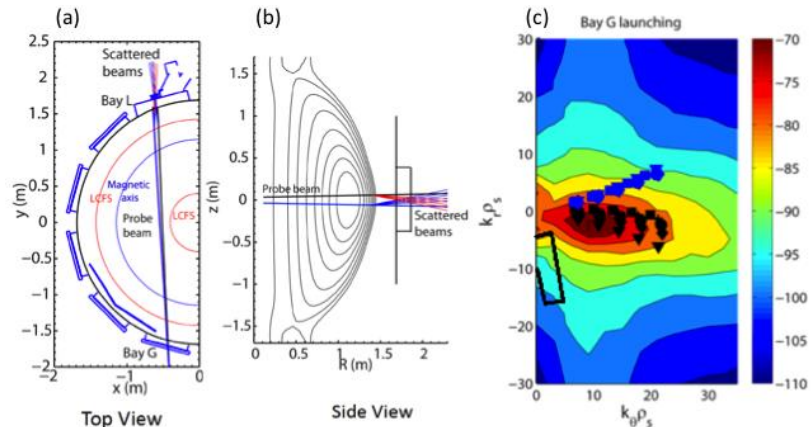


Fig. 10.41. High-k scattering system with two scattering schemes. (a) Schematic of the toroidal cross section of the high-k scattering beam geometry. (b) Poloidal cross sectional view of the beam geometry. (c) Regions in 2D k - r and k - θ space covered by two scattering schemes.

high- k scattering system mainly relies (as did the previous system) on the large magnetic shear in NSTX-U to provide radial localization. The simulation is performed using predicted profiles for a high-performance NSTX-U H-mode plasma. The anisotropy in the 2D k -spectrum of ETG turbulence, i.e. the existence of ETG streamers, can be determined by comparing the k -spectrum measured by the different schemes. Furthermore, a range of k_θ and k_r can be scanned by varying launching and receiving optics to map a wide range of 2D k -spectrum. An example of the scattering geometries and 2D k -spectrum of turbulence is shown in Fig. 10.41(c).

10.6.2.2. Beam Emission Spectroscopy

The Beam Emission Spectroscopy (BES) diagnostic on NSTX-U, based upon observing the $D\alpha$ emission of collisionally-excited neutral beam particles, will enable direct spatially-resolved measurements of

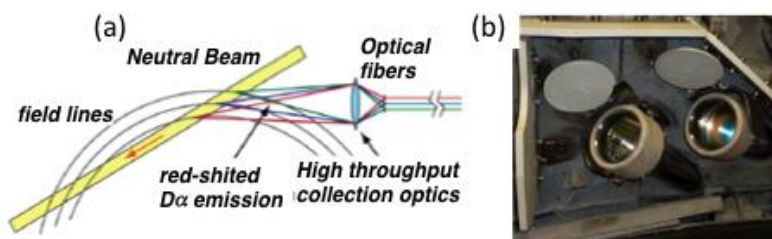


Fig. 10.42. Beam Emission Spectroscopy. (a) A schematic of BES diagnostic system. (b) BES collection optics placed in NSTX-U.

longer wavelength density fluctuations in the plasma core, providing valuable insights into the suppression of ion turbulence and the attainment of near-neoclassical ion confinement on NSTX-U [23]. The BES diagnostic together with the existing microwave tangential scattering diagnostic (which measures medium to short wavelength turbulence) will provide the most comprehensive turbulence diagnostic set available. The BES diagnostic also enhances measurements of the spatial structure of fast-ion-driven instabilities such as the TAE and BAAE observed on NSTX. BES measurements therefore contribute to several NSTX-U research areas, including turbulence and transport, waves and energetic particles, and boundary physics. Specific scientific applications include investigations of turbulence, turbulent flows, zonal flows, energetic particle modes, and Edge Localized Modes. University of Wisconsin has previously developed an advanced 24-channel Beam Emission Spectroscopy (BES) diagnostic system on NSTX. A schematic of the BES system layout and the collection optics installed inside of the NSTX-U vacuum chamber are shown in Fig. 10.42, respectively. For NSTX-U, an expansion of BES to 48 detection channels will be implemented to improve the scientific productivity of the BES system on NSTX-U. Initial BES measurements on NSTX have identified the general characteristics of long-wavelength turbulence in NSTX plasmas. BES point spread function calculations will be developed to apply BES synthetic diagnostics to simulation results.

10.6.2.3. Microwave Polarimeter Magnetic Fluctuation Diagnostic

UCLA recently completed development of a sensitive $\sim 300\text{GHz}$ radially-viewing polarimeter to directly measure magnetic field fluctuations in NSTX-U [24]. The polarimeter has been installed on DIII-D in preparation for NSTX-U. DIII-D plasmas are well-suited since operation at magnetic fields (0.5 – 1T) is practical and consistent with NSTX-U. NTM, fast-ion driven mode and microtearing simulations will be utilized to assess feasibility and interpret polarimetry measurement of magnetic fluctuations. Experimental data in conjunction with predicted mode structure will be used to validate simulation codes. It is expected that magnetic fluctuation levels $B_{\sim} / B \sim 0.01\%$ will be observable.

10.6.2.4. Gas Puff Imaging Diagnostic

The gas puff imaging (GPI) diagnostic was operated successfully on NSTX from 2000 to 2010, and the existing GPI hardware from 2010 will be reinstalled on NSTX-U at the same location (Bay B) [25]. This diagnostic viewed the 2-D structure of edge turbulence near the outer midplane and provided detailed data on the physics of L-H transitions, zonal flows, blob dynamics, and ELMs. It is planned to add one or more additional GPI views in order to clarify the full 3-D structure of edge turbulence, which is crucial for understanding edge and SOL transport. One of these views would be in the lower divertor region, where interesting turbulent structures have already been seen using (passive) imaging of LiI light. New GPI views at other toroidal and poloidal angles are also desirable to understand the formation process of blobs (which determine the scrape-off layer width) and the structure of zonal flows (which may be important for the L-H transition). In addition, there are interesting interactions between RF waves and the SOL on NSTX which can be studied with GPI at the RF antenna structure. These additional GPI views can be implemented using in-vessel fiber optic bundles and telescopes, as previously done for the GPI diagnostic on C-Mod.

10.6.3. MHD / ASC Diagnostics

For advanced ST operations, it may be necessary to control the pressure and plasma current profiles which would require real time measurements of plasma pressure and current profiles. The JHU group is installing 96 channel edge and core tangential multi-energy-soft-x-ray arrays for fast time scale plasma profile measurements (10.6.1.3). Nova Photonics is implementing real time MSE which can give the real time plasma current profile information in addition to the MSE-CIF (10.6.1.4) and MSE-LIF (10.6.1.5) systems.

10.6.3.1. Magnetics For Equilibrium Reconstruction, Boundary Control, and RWM Suppression

NSTX had a comprehensive set of magnetic diagnostics, including ~ 45 poloidal flux loops, ~ 60 magnetic field sensors for constraining equilibrium reconstruction codes such as EFIT, and 48 in-vessel sensors for measuring and controlling resistive wall modes [26]. These sensor systems will be retained on NSTX-U, but with some significant improvements. In particular, the density of poloidal magnetic field probes flux loops in the divertor region will be increased, in anticipation of improving the magnetic reconstruction of snowflake divertor configurations. Furthermore, a second vertical array of poloidal field sensors will be installed on the center column, increasing the redundancy of these critical measurements. Finally, the density of poloidal magnetic flux loops in the vicinity of the divertor coil mandrels will be increased, allowing better reconstruction of the eddy currents induced in these support structures.

10.6.3.2. Real-Time Velocity Diagnostic

A Real-Time Velocity (RTV) diagnostic was installed on NSTX to measure the plasma toroidal velocity with high temporal resolution [27]. The real-time velocity data will be incorporated into the plasma control system for feedback control of the plasma rotation profile using the NBI systems and non-resonant magnetic braking using the 3-D control coils (10.5.1) as the actuators.

The RTV system, based on active charge-exchange recombination spectroscopy (CHERS), can measure at up to six radial locations with a maximum sampling rate of 5 kHz. The RTV system uses two toroidally separated views to distinguish the CVI emission from the region intercepting the heating NB from the background (intrinsic) contribution. The system uses fixed-wavelength spectrometers coupled to fast CCD cameras to provide the high sampling rate needed for real-time control. Acquisition of camera data by a computer and its analysis within a total time interval under 200 μ s, including the read-out, background subtraction and fitting of multiple Gaussian components to the measured line shape, was demonstrated. A scheme for conveying the analyzed data to the NSTX-U plasma control system using its existing data acquisition hardware was developed and tested. The spectrometer wavelength

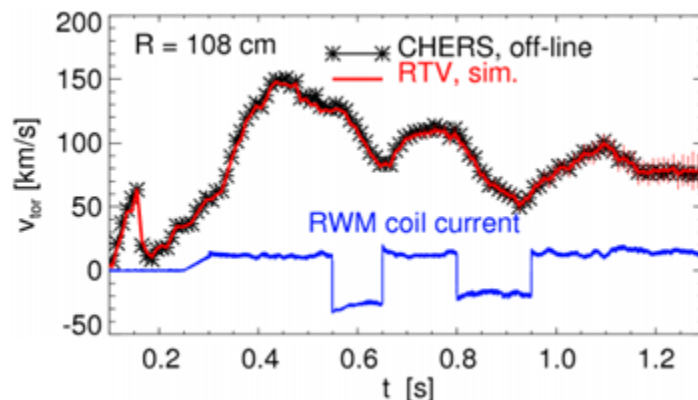


Fig. 10.43. Successful algorithm test of real-time toroidal velocity measurement in NSTX.

calibration was established by observing spectral lines close in wavelength to the CVI line from a neon glow discharge run in the NSTX vacuum chamber. A real-time velocity diagnostic, which is integral to macroscopic stability research because of its use in rotation control and disruption detection, has already been installed and successfully tested in NSTX as shown in Fig. 10.43.

10.6.3.3. Real time MSE (rtMSE)

High performance commodity computers have become fast enough to handle the real-time computing requirements needed for rtMSE [28]. We propose to use a fast quad core server running a modified version of the Linux operation system that is used for the NSTX PCS (10.3.3.3). The OS modifications allow for real-time operations and will be coordinated with the computing group on NSTX-U. The digitizer hardware needs to be chosen carefully for compatibility. Equipment from National Instruments and D-Tacq is under consideration. The NI digitizers are more attractive from a hardware perspective, as they are based on the newer PXIe (PXI express) format, which has a very high streaming bandwidth with low latencies. Since MSE derives the pitch angle from a carrier signal at is that National approximately 44 kHz, the digitization rate we currently use is 800 kSamples/s. High density modules suitable for MSE are readily available from NI. However, driver support in Linux needs to be investigated. An encouraging development, NI has begun supporting the PXIe series of digitizers with their MHDDK (Measurement Hardware Driver Development Kit), which allows for custom driver development in Linux at the register level. Another possibility is to use D-Tacq (<http://www.d-tacq.com>) digitizers, which have already been adapted for use with the custom Linux in question at multiple fusion experiments, including DIII-D, C-Mod, and EAST. In the near term, a suitable digital lock-in will be developed in a language to perform real-time analysis. The MSE pitch angles need to be transmitted to the NSTX-U PCS software. The NSTX-U PCS team will be integrating the rtMSE data into the PCS system via the real-time reconstruction program rtEFIT.

10.6.3.4. Real-Time Multi-Pulse Thomson Scattering (rtMPTS)

The MPTS diagnostic can be modified to supply inputs to the real-time plasma control system (PCS) [29]. An initial step for real-time MPTS (rtMPTS) would be to use existing buffered outputs of the multiplexed raw-data signal as input for a rapid – real-time – calculation of T_e and n_e , for a subset of the existing 42 radial channels. The resulting data would be transferred to PCS in numeric or analog form, as needed. The current two-laser configuration provides a 16.7ms time resolution; the implementation of a third laser would reduce this number to 11.1ms. An advantage of using the buffered outputs mentioned above is that the normal flow of the CAMAC based data acquisition will not be interrupted or compromised, but it comes with an intrinsic latency of 0.4ms.

Using PXI (Peripheral Component Interconnect) electronics or equivalent, one could expect an overall latency of the order of 1ms. The rtMPTS electronics and computer would be located in the polychromator room. A more direct access to the preamplifier outputs would reduce latency at the cost of greater complexity. On the other hand a replacement of the CAMAC data acquisition is clearly needed and at such time attention will be given to the needs of rtMPTS. It might be possible to have all MPTS radial channels available for rtMPTS. In its simplest form rtMPTS could provide two radial channels data: center and edge. But a likely PCS need will be real-time line average density in which case at least ten MPTS radial channels would be needed. In a more advanced scenario, profile information from rtMPTS would be used for real-time equilibrium calculation based on isobaric (p_e) isobaric or isotherm (T_e) isotherm flux surfaces. Such calculation are routinely made in “between shots” analyses, *e.g.* isobaric EFIT02 and isotherm LRDFIT04.

10.6.3.5. Real-Time Density Interferometry

The far infrared tangential interferometer/polarimeter (FIRETIP) has operated reliably in providing line-integrated density measurements on NSTX. Its feasibility for real-time density control has been investigated [30]. Fringe jumps that have been prohibiting the plasma density from use in the direct feedback to actuators have been suppressed. A conceptual design of a density feedback control system including the FIRETIP, control hardware, and software that takes advantage of the NSTX-U plasma control system (PCS) has been developed. It can be used as the basis for a density feedback control system on NSTX-U. A central FIRETIP sightline is to be implemented initially for this purpose. Fringe jumps in the FIRETIP were well characterized using data obtained with new fast electronics prior to the end of NSTX operations. The algorithms used to suppress the density errors they caused were shown to work properly through comparisons with the Thomson scattering diagnostic. The fringe jump correction algorithm, as well as safety and feedback modules, can be included as part of the PCS effort for NSTX-U.

10.6.3.6. Diagnostics for disruption mitigation experiments

Toakamak disruption mitigation experiments have shown that the dissipation of plasma energy usually consists of two distinct phases: (a) the thermal quench in which plasma loses most of its thermal energy ($\Delta t \sim 1$ ms), and (b) the current quench during which the cold plasma slowly dissipates the stored magnetic energy ($\Delta t \leq 10$ ms). During the thermal quench phase on NSTX, the fast dynamics of the hot plasma ($T_e > 1$ keV) can be diagnosed using a collection of soft X-ray (SXR) diagnostics (see 10.6.1.3). The SXR diagnostic suite will be a valuable tool in understanding the role of impurity dynamics during the thermal quench and disruption evolution. Additionally, detailed SXR

measurements of intrinsic impurity concentrations will be used to validate simulation results which can show significant discrepancies in edge plasma densities and impurity levels. ME-SXR measurements on NSTX-U will also provide T_e profile data for the dynamic plasma cooling during a disruption thermal quench, and hence provide quantitative estimates of the large perpendicular heat transport (χ_{\perp}) [31].

The current quench phase of the tokamak disruption is generally more difficult to diagnose using SXR measurements due to the low electron temperature (\sim few eV) of the plasma. Therefore, the JHU

group plans to develop a novel, fast XUV 2D imaging radiometer which will measure impurity dynamics and spectrally resolved radiated power during the current quench.

This diagnostic design is based on previous transmission grating instruments built by the JHU group, with the

advanced 2D diode detector providing fast (\sim 10kHz) spatially and spectrally resolved XUV impurity emission measurements (Fig. 10.44) [32]. Like previous TG spectrometers, the fast 2D disruption radiometer uses an imaging slit coupled to a freestanding transmission grating to produce spectrally resolved one dimensional images of the plasma on the 2D diode array detector. The 2D diode detector will measure the impurity line radiation during current quench phase in the XUV range (200-1400Å), with enough SNR to measure the spectra with a rate of \sim 20 kHz.

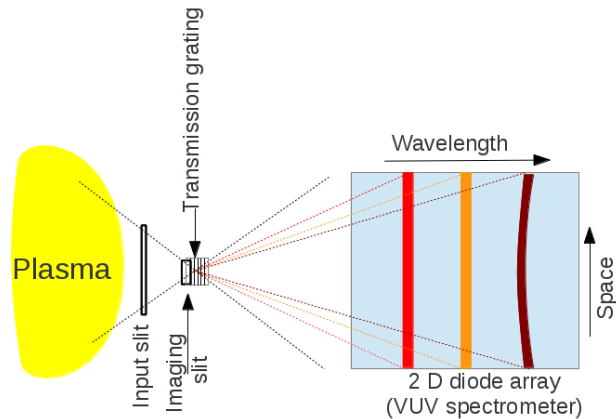


Fig. 10.44. Schematic of TG disruption radiometer.

10.6.4. Boundary Physics Diagnostics

The NSTX/NSTX-U facility has been investing strongly in boundary physics related diagnostics in the past several years. Some of the recently implemented PMI diagnostics which will be available for Day 1 on NSTX-U are shown in Fig. 10.45. There are over 20 PMI and edge plasma diagnostic systems on NSTX-U and additional ones are being readied. They include Gas-puff Imaging (500kHz), Langmuir probe array [33],

Edge Rotation Diagnostics (T_i , V_ϕ , V_{pol}), 1-D CCD H_α cameras (divertor, midplane), 2-D fast visible cameras for divertor and overall plasma imaging [34], Divertor bolometer, IR cameras (30Hz), Fast IR camera (two color), Tile temperature thermocouple array, Divertor fast eroding thermocouple, Dust detector, Quartz Microbalance Deposition Monitors, Scrape-off layer reflectometer, Edge neutral pressure gauges, Material Analysis and Particle Probe, Divertor Imaging Spectrometer, Lyman Alpha (Ly_α) Diode Array, Visible bremsstrahlung radiometer, Visible and UV survey spectrometers, VUV transmission grating spectrometer, Visible filterscopes (hydrogen & impurity lines), and Wall coupon analysis. Major upgraded boundary physics diagnostics are described in more detail below.

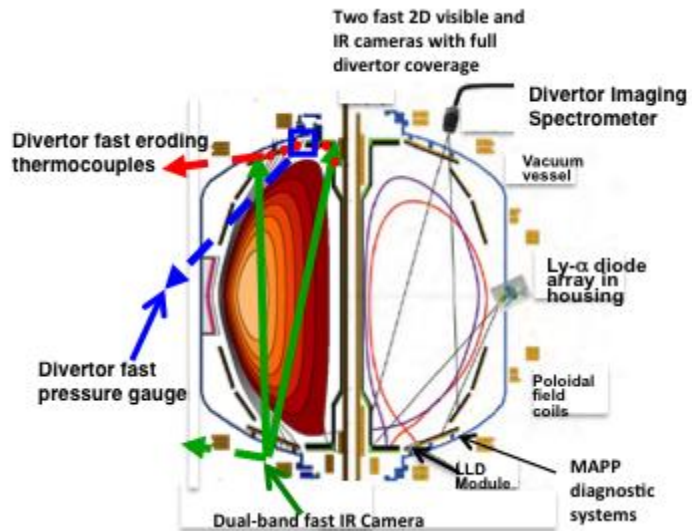


Fig. 10.45. Initial divertor diagnostics for NSTX-U.

10.6.4.1. Material Analysis Particle Probe (MAPP)

A major NSTX-U PMI diagnostic addition is the Material Analysis Particle Probe (MAPP) by Purdue University as shown in Fig. 10.46 (a) [35]. MAPP is an in-vacuo inter-shot diagnostic capable of correlating surface chemistry evolution with plasma response to PMI conditioning. MAPP utilizes multiple surface-science measurement techniques to characterize a sample material exposed to NSTX-U conditions and assess plasma-surface interactions near the divertor strike point. A unique sample head has been designed for MAPP to allow simultaneous exposure of up to four samples to plasma discharges [see Fig. 10.46(b)]. The surface of each sample is positioned (via shims or custom machining) colinear to the top surface of the retaining stems in order to avoid self sputtering.

Independently controlled heaters are contained beneath each sample and radiative and conductive cross-talk heating is reduced using perforated sample stems and vertical heat baffle shields. Following plasma exposure, samples are retracted *in-vacuo* into an adjoining chamber, where a variety of analysis techniques are performed during the in-between shot window. Analysis techniques include X-ray photoelectron spectroscopy (XPS) – used to assess the chemical interactions of the top ~10 nm, ion scattering spectroscopy (ISS) – interrogates the top 1-2 monolayers to determine surface chemical composition, and direct recoil spectroscopy (DRS) – uniquely capable of measuring the surface hydrogen content in samples. In addition, thermal desorption spectroscopy (TDS) can be performed at the end of each day in order to measure and quantify bulk deuterium retention.

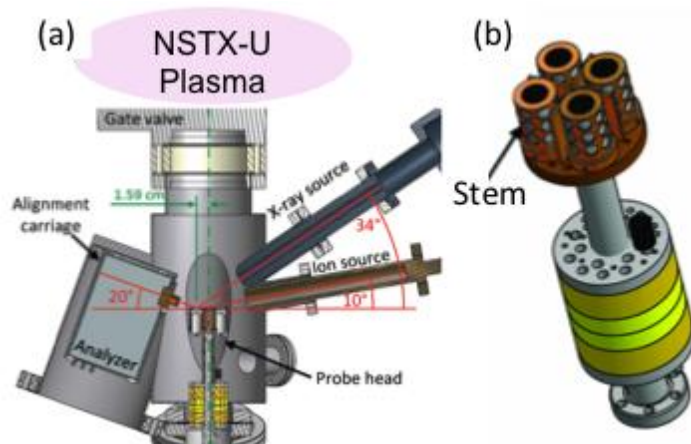


Fig. 10.46. MAPP System (a) Schematic of MAPP system. (b) A schematic of MAPP sample head.

10.6.4.2. Divertor Spectrometers and Two-Color Fast Infrared Camera

The LLNL collaboration in the divertor diagnostics area on NSTX focused on new and improved measurements for plasma-surface interaction studies with lithium-coated graphite and molybdenum plasma-facing component, as well as divertor impurity and plasma diagnostics. New capabilities included a new vacuum-ultraviolet divertor spectrometer (SPRED) that was brought from LLNL to NSTX-U to monitor carbon and molybdenum emission in the divertor for impurity and power balance studies [36, 10.37]. Another new capability intended to support the NSTX-U lithium program is a new near-infrared spectrometer for divertor molecular and atomic spectroscopy. To provide pilot measurements for radiative divertor control, a new optical Penning discharge chamber is installed in the lower divertor area to provide a way to monitor pressure of deuterium or or gaseous impurities (e.g., argon) that could be injected to increase divertor radiated power. Improvements were also made to other LLNL-supported diagnostics, notably the divertor Lyman-alpha and radiometer array, four one-dimensional filtered CCD arrays, divertor imaging spectrometers, and filterscopes. The goal was to provide routine quantitative emission measurements in the upper and lower divertor areas, as well as the inner outer walls.

Another important divertor diagnostic recently developed is a two-color or dual-band device developed for application to high-speed IR thermography by ORNL [38]. Temperature measurement with two-band infrared imaging has the advantage of being mostly independent of surface emissivity, which may vary significantly for an LLD as compared to that of an all-carbon first wall. In order to take advantage of the high-speed capability of the existing IR camera (1.6-6.2 kHz frame rate), a commercial visible-range optical splitter was extensively modified to operate in the medium wavelength (MWIR) and long wavelength IR (LWIR). This two-band IR adapter utilizes a dichroic beamsplitter which reflects 4-6 micron wavelengths and transmits 7-10 micron wavelength radiation, each with $> 95\%$ efficiency and projects each IR channel image side-by-side on the camera's detector. The ORNL boundary physics group has designed and implemented a wide angle, 30 Hz infrared camera system on NSTX in FY 2011. A dual-band adapter was also implemented for variable surface emissivity due to lithium films. This system was designed as part of Princeton University student's first year experimental project. In addition, two eroding thermocouples near the PFC tile surface were installed and instrumented. These thermocouples, which have a design response time ~ 1 ms are intended to be used in the future for feedback control of PFC surface temperature in NSTX-U. Finally a set of 16 new "filterscope" chords were implemented. The gain control and data acquisition is done dynamically via PC. The units are capable of 100 kHz sampling speeds.

A Divertor Imaging Radiometer for spectrally resolved measurements of the radiated power by Johns Hopkins will extend the multi-energy concept to divertor diagnostic by performing absolute measurements of the radiated power in tens of spectral bins covering the range from several eV to few hundred eV (VUV to XUV). The radiometer will use dual transmission gratings in conjunction with a direct detection CCD camera and will view the divertor from the outboard side, with vertically spaced lines of sight from the X-point region to the strike-point region. The instrument will have ≥ 2 cm space resolution and ≥ 10 ms time resolution. The proposed diagnostic will provide, for the first time in a tokamak, measurements of the spectrally resolved radiated power from the divertor and will enable determination of the radiating impurity type and charge state distribution over the range of temperatures expected for the NSTX-U divertor. This in turn will provide information on the radiating efficiency and transport of *injected* impurities for radiative divertor studies, as well as information on *intrinsic* impurities and associated radiation. In addition, the proposed diagnostic will be used to calibrate and validate the advanced divertor modeling codes used at NSTX-U. We will also study using the radiometer in conjunction with divertor emission modeling for a spectroscopic diagnostic of the electron temperature and cross-field particle transport in the divertor. Even if approximate, such measurements will be useful for the NSTX-U divertor research.

10.6.4.3. Dust Detector and Quartz Crystal Microbalances

Another novel PMI diagnostic is the first real-time detection of surface dust inside a tokamak that was made using an electrostatic dust detector [39]. As shown in Fig. 6(a), a fine grid with 25 μm spacing of interlocking circuit traces was installed in the NSTX-U vessel and biased to 50 V. Impinging dust particles created a temporary short circuit and the resulting current pulse was recorded by counting electronics. Various techniques were used to increase the detector sensitivity by a factor of 10,000 to match NSTX-U dust levels while suppressing electrical pickup. The results were validated by comparison to laboratory measurements, by the null signal from a covered detector that was only sensitive to pickup, and by the dramatic increase in signal when Li particles were introduced for wall conditioning purposes. It should be noted that the real time dust measurement is necessary to safely manage the dust generated in ITER. Dynamic retention of deuterium, lithium deposition, and the stability of thick deposited layers were measured by three quartz crystal microbalances (QMB) deployed in plasma shadowed areas at the upper and lower divertor and outboard midplane. Deposition of 185 $\mu\text{g}/\text{cm}^2$ over 3 months in 2007 was measured by a QMB at the lower divertor while a QMB on the upper divertor, that was shadowed from the evaporator, received an order of magnitude less deposition. Occasionally strong variations in the QMB frequency of thick lithium films were observed suggesting relaxation of mechanical stress and/or flaking or peeling of the deposited layers.

10.6.4.4. Divertor Thomson Scattering System

Understanding divertor heat and particle transport in the advanced divertor configurations is a necessary first step toward their performance optimization. Also understanding the linkages between the midplane SOL and divertor is very important for ITER and the design of future fusion devices. An effort is underway by the LLNL group to develop a conceptual design of the Divertor Thomson Scattering (DTS) system in NSTX-U [40]. The DTS system would not only support the planned advanced and radiative divertor studies, but would also enable unique physics studies of the lithium coated plasma facing components, ELM transport in the divertor, and many others.

In combination with the additional midplane SOL Thomson scattering channels in the SOL, the DTS system would provide unique two-point T_e and n_e profile measurements upstream and downstream of the divertor X-point region that would allow critical tests of SOL heat and particle transport models. Implementation of DTS is a large technical effort that involves various personnel skills, e.g. physics, engineers, technicians, safety engineers, as well as a wide range of work activities: mechanical and optical engineering and design, diagnostic assembly, and facility integration. The latter alone is a large effort which would require designing and fabricating three new ports on the NSTX-U vacuum vessel, their metrology and safety. The LLNL activities in the area of conceptual design are summarized as follows. LLNL personnel have been involved in operation of the DIII-D DTS since the beginning of 2012. Valuable experience has been gained from hands-on maintenance, alignment, and design of upgrades. A beam schematic of a possible divertor Thomson scattering system is shown in Fig. 10.47. LLNL have also identified possible laser beam and collection optics placement and viewing geometries using the NSTX-U center stack and vacuum vessel models.

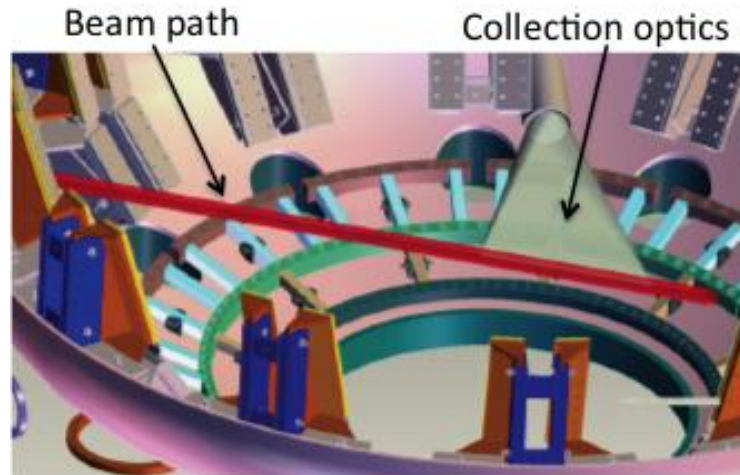


Fig. 10.47. Divertor Thomson Scattering geometry proposed for NSTX-U

10.6.5. Energetic Particle Diagnostics

In the energetic particle (EP) research area, in addition to the perpendicular and newly implemented tangential fast ion D-alpha (FIDA) diagnostics, additional SSNPA (Solid-State Neutral Particle Analyzer) channels will be implemented since the scanning NPA was removed. Additional diagnostics for EP studies on NSTX-U include neutron rate counters, a scintillator-based Fast Lost-Ion Probe (sFLIP), installed on the vessel wall, and a new charged fusion product (CFP) profile diagnostic. The 16 channel reflectometry will be also installed for the energetic particle mode measurements.

10.6.5.1. Energetic Particle Distribution Diagnostics

On NSTX-U the radial fast ion profile is characterized through the FIDA and ssNPA systems. A vertical FIDA system [41] measures fast ions with small pitch, corresponding to trapped or barely passing (co-going) particles. A new tangential FIDA system [42] (Fig. 10.48) measures co-passing fast ions with pitch ~ 0.4 at the magnetic axis up to 1 at the plasma edge. Both FIDA systems have time resolution of 10 ms, spatial resolution ≈ 5 cm and energy resolution ≈ 10 keV. An upgraded solid-state Neutral Particle Analyzer [43] (ssNPA) will provide energy-integrated measurement of trapped fast ions, with a lower energy threshold $E_{min} \sim 20$ keV, from 5 radii. The ssNPA system will mainly work in current-mode to get fast time response. The sampling rate is ≈ 1 MHz. Two ssNPA channels will also incorporate pulse-counting mode capability to obtain energy spectra with ~ 10 keV energy resolution and ~ 10 ms temporal

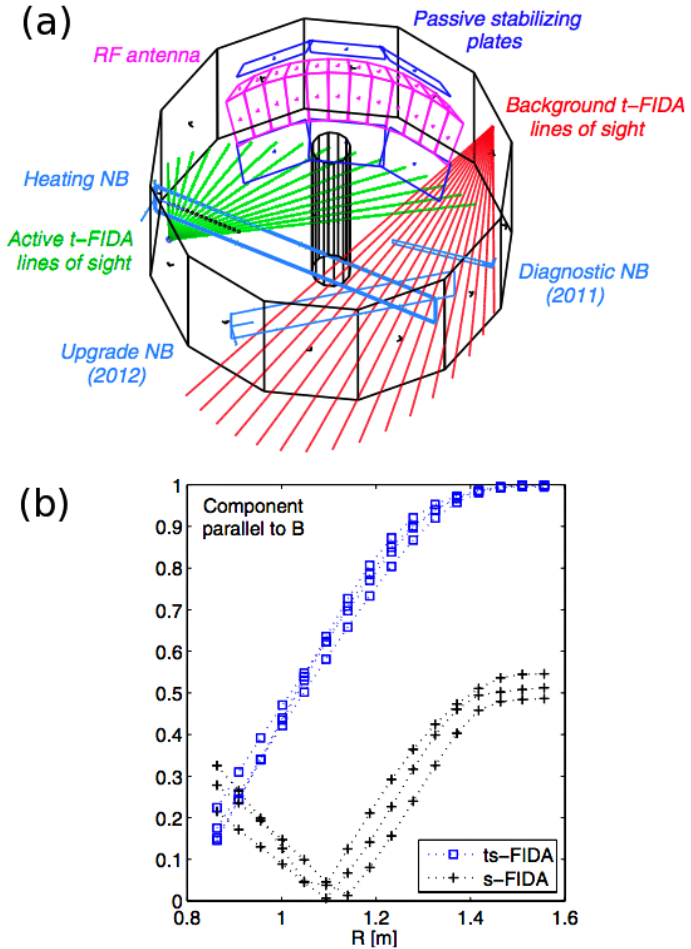


Figure 10.48. (a) Layout of the new tangential FIDA system. (b) Expected component parallel to the magnetic field for the tangential (ts-FIDA) and vertical (s-FIDA) FIDA systems. A value of 1 (0) on the y axis corresponds to a parallel (perpendicular) view.

resolution. The fast-ion distribution function F is a complicated function of energy, pitch angle, space, and time. Successful reconstruction of F requires multiple measurements with a variety of techniques.

In hardware, UC Irvine will concentrate on four active beam measurements: vertical FIDA, tangential FIDA, E||B NPA, and SSNPA. In analysis, we will develop software that uses these and other fast-ion diagnostics to infer the fast-ion distribution function from the data. Inverted distributions will be compared with calculations by theoretical collaborators. The vertical FIDA system is a working diagnostic that has been producing valuable data for several years. Only minor changes to this diagnostic are proposed. The tangential FIDA system is patterned after the vertical FIDA diagnostic. Although it has not collected data during plasma operations, its installation is essentially complete. The SSNPA diagnostic will be displaced from its present location by the new beam-line. A new SSNPA diagnostic will be designed and installed to measure trapped fast ions at several radial locations.

Spectral information from FIDA is complemented by data from a NPA system at a fixed radius. The excellent spectral resolution of the NPA is required for careful validation of NUBEAM predictions. The neutral particle analyzer (NPA) in use on NSTX [42] utilizes a E||B (superimposed parallel electric and magnetic fields) spectrometer developed at PPPL that simultaneously measures the mass-resolved energy spectra of both H and D neutrals with a time resolution of ~ 0.1 ms, set by signal-to-noise levels. A multi-anode micro-channel plate detector provides 35 energy measurements for each species with an energy dynamic range of $E_{\max}/E_{\min}=30$. The tunable energy range is $E_H=1-600$ keV, $E_D=1-300$ keV and the energy resolution varies over a range of $\Delta E/E=2-5\%$, moving from high to low energy. Intersection of the E||B NPA sightline with the neutral beam footprint enabled localization of measurements to the plasma core region. The primary applications of the E||B NPA on NSTX have been measurement of fast ion redistribution and/or loss due to wave-particle interactions that are driven by MHD activity and the characterization of fast ion response to HHFW injection.

Additional diagnostics for EP studies on NSTX-U include neutron rate counters, a new charged fusion product (CFP) profile diagnostic and a scintillator-based Fast Lost Ion probe (sFLIP), installed on the vessel wall. Neutron counters are strongly weighted toward the higher-energy portion of the distribution function, with no pitch dependence. For example, an increased count rate during HHFW injection is a straightforward indicator of the formation of tails in the fast ion distribution above the NB injection energy. In addition to the volume-integrated detectors that were already available on NSTX-U, a set of 4 collimated neutron detectors is being considered for installation in

Year 3 (pending incremental funding). These additional measurements can be integrated in the TRANSP code for improved constraints on the simulated neutron rate.

Similarly to neutron counters, the CFP diagnostic would provide direct measurements of the fusion reactivity [45]. Because both protons and tritons are largely unconfined for NSTX-U parameters, fusion products are eventually detected outside the plasma volume. By knowing the magnetic field geometry, their orbit can be tracked back in the plasma. Such orbits are equivalent to curved sightlines for each detector, so that multiple signals can be inverted to infer a radial profile of the high-energy fast ions. A 4-channel CFP prototype will be tested in FY-13 on the MAST device, then a 8-channel (possibly upgraded to 16 channels) system will be ready for installation on NSTX-U in FY-14. Target performance is 1-2 ms temporal resolution for fusion reactivity levels comparable with the NSTX-U values.

A scintillator-based Fast Lost Ion probe (sFLIP) contributes to the NB characterization by providing energy and pitch resolved spectra of lost fast ions, e.g. from prompt losses, as the NB tangency radius is varied. sFLIP is being upgraded with a faster CCD detector capable of frame rates up to 100 kHz [46]. A set of photo-multiplier tubes is also being installed on sFLIP for energy and pitch integrated measurements at rates up to 250 kHz from 6-10 sub-regions of the sFLIP scintillator plate.

10.6.5.2 Energetic-Particle-Induced Mode Diagnostics

A recently-developed, UCLA 16-channel comb quadrature reflectometry system has been utilized on NSTX to study the eigenmode structure of fast-ion driven Alfvén as well as other MHD modes [47]. This unique system has also provided a wealth of additional information including investigation of three-wave coupling processes and identification of the potential role of Compressional Alfvén Eigenmodes (CAEs) in contributing to core anomalous transport. In order to prepare for higher density operation in NSTX-U it is proposed to expand operation to 100GHz through the installation of 8 additional channels. This upgrade to 24 channels will allow detailed eigenmode structure measurements in high performance NSTX-U plasmas.

Similarly to NSTX, several arrays of high-frequency Mirnov coils will provide routine measurements of the fluctuations spectrum on NSTX-U. Two sets of coils are toroidally displaced to enable the computation of the toroidal mode number of the modes from the phase of the complex spectrum. A reduced set of coils is displaced poloidally to provide information on the poloidal mode structure. The bandwidth of the magnetic fluctuation measurements will be extended on NSTX-U from the present 2-2.5 MHz up to 4 MHz, to

account for the expected frequency up-shift of the modes as the toroidal field is increased.

Another quantity of great relevance for EP studies is the radial structure of *AE modes. Several complementary systems will be available to this end on NSTX-U, including beam emission spectroscopy (BES) arrays, reflectometers, interferometers, polarimeters, and X-ray detectors. A proposal for installing a Doppler back-scattering (DBS) system will be also considered based on the available funds (see below).

The BES system (as described in Sec.10.6.2.2.) will provide low-k density fluctuation measurements near the mid-plane for normalized radii $0.1 < r/a < 1$. The number of channels will be increased from 32 up to 64 to simultaneously sample a wide region of the plasma. The measurement region will extend poloidally to cover a ~ 10 cm broad strip along the mid-plane. Further improvements may include a toroidally-displaced set of viewing channels, possibly limited to the edge region, to measure background emission (in the absence of the 2nd NB source) or the toroidal mode number of the instabilities.

Density fluctuations are also derived from a multi-channel reflectometer system. The 16 channels available on NSTX will be complemented by 8 new channels at higher frequency, which will enable fluctuation measurements up to densities $\sim 10^{20} \text{ m}^{-3}$. Line-integrated measurements of density fluctuations will also be available from 3-4 far-infrared interferometer with sampling frequency ~ 4 MHz.

Beside density fluctuations, other quantities such as magnetic field and velocity fluctuations are important for a thorough identification and characterization of the different instabilities. A new radial polarimeter system will provide direct measurement of magnetic fluctuations along the mid-plane. Pending incremental funding for diagnostics development, flow fluctuations will be measured through a millimeter-wave Doppler back-scattering (DBS) system operating in the 80-100 GHz frequency range. This new measurement capability represents an alternative, substantially independent tool for identifying fast-ion modes that would significantly strengthen comparison with theory, expanding previous internal measurements of fast-ion modes previously restricted to perturbed density on NSTX.

Additional information on fluctuations with frequency < 100 kHz will be provided by a multi-energy SXR array with two toroidally displaced sets of views. Spatial resolution varies from ~ 1 cm at the outboard mid-plane ($R > 150$ cm) to ~ 3 cm in the core and inboard mid-plane region ($40 < R < 140$ cm) (see Fig. 10.38). Faster measurements with up to ~ 500 MHz bandwidth will be available from a system of two poloidal SXR arrays.

Each array contains 16 channels viewing poloidally through two variable selected filters, with 2-3 cm resolution.

10.6.5.3. Alfvén Eigenmode Antenna for AE Stability Measurements

Simple antennae have been used in several machines (JET, C-Mod) to study TAE stability. The linear damping rate can be measured by sweeping the antenna frequency through the mode frequency. It will be useful to extend these studies to low aspect ratio tokamaks (MAST and NSTX). This would also help to validate ITER projections by challenging our fundamental understanding of the physics in the drive and stability of these modes. For low aspect ratio the antenna can also be used to study higher frequency Alfvén modes such as GAE and CAE.

The “MHD active spectroscopy” plan begins with relatively simple antenna design. As operational experience builds up, more ambitious designs will be tried. In years 1&2 several proto-type antenna designs will be evaluated to optimize the coupling to TAE and CAE. The NSTX-U prototype AE antenna system consists of up to 4 compact modules, each of which is a single, 5-turn ‘window-frame’ coil, similar in principle to those used on JET, C-Mod and MAST. In parallel, the external power supplies for driving the antenna, the coupling networks and control hardware and software will be developed. While the highest priority will be to develop the capability to study TAE, some time will be devoted to evaluating the antenna and coupling network at frequencies up to 2MHz, as will eventually be needed for Global and Compressional Alfvén eigenmode studies.

Pending incremental funding, in Years 3-5 there will be the opportunity for continued improvement of *AE antenna designs and perhaps amplifier upgrades. Additional coils will allow for improved selectivity of the toroidal mode number, as well as improving the coupling of the antenna to the modes. However, particularly in years three and four there will an emphasis on designing experiments to measure TAE linear damping rates under as broad a range of conditions as possible. The low power ($\approx 1\text{kW}$) experiments will provide important information on antenna coupling and natural damping rates for each of the eigenmodes. This information will be used to determine the potential benefits of higher power experiments. If the natural eigenmode damping rates are small, there is the possibility of driving them to amplitudes where stochastic heating of thermal ions occurs.

10.7. NSTX-U Plasma Operation Start-Up Plan

Making the transition from engineering project management to operations engineering requires certain considerations. For example, sound project management will lead to the successful completion of a system to all of its technical requirements, but may not consider important concerns such as that system's operation in concert with other systems, staging the pre-operational and subsequent integrated system testing, establishing and controlling interrelated subsystem operating limits, maintaining interrelated safety interlock and equipment protection circuitry, maintaining configuration control during repairs/maintenance, proper analysis of hazards before beginning work, training and work authorizations for engineers/operators/technicians, managing personnel access to the various experimental areas, defining expected personnel conduct while in these areas, and managing temporary modifications.

The NSTX-U project has addressed the above considerations with a network of administrative and technical procedures to assign operational roles, coordinate operations-related activities and machine configurations, and maintain a safe work environment. This includes the authorization of allowable operating parameters for a given machine configuration, and the system for the establishment/testing of all coil protection systems for those parameters.

The NSTX-U integrated system testing, commissioning, and start-up will follow the same process as the NSTX initial start-up in 1999, and each subsequent return to operations after an extended outage where machine upgrades were implemented. There are four components to NSTX-U post-construction start-up:

1. Activity Certification Committee (ACC) Review
2. Operational Readiness Assessment (ORA)
3. Completion of sub-system preoperational testing (PTP's)
4. Run start-up procedure (OP-NSTX-02) including integrated system testing (ISTP)

The NSTX-U Activity Certification Committee (ACC), comprised of representatives from PPPL Engineering, Physics, Safety, and the DOE Princeton Area Office (PAO), reviews newly installed sub-systems and collateral devices with regard to personnel, environmental, and machine safety. The ACC will perform physical walk-downs of equipment and document reviews in developing a findings report to be submitted to the PPPL Deputy Director of Operations and the NSTX-U Operations Manager. After submittal of the ACC report and any associated open items, non-compliances or safety concerns, the PAO will conduct an Operational Readiness Assessment (ORA) before the project may move to start-up.

By this time, the sub-system cognizant engineers will have developed and are performing their pre-operational test procedures (PTP's). The NSTX-U Start-Up procedure (OP-NSTX-02) will coordinate and document the completion of the various sub-system PTP's, interlock and equipment protection test procedures, and all safety system checks. OP-NSTX-02 concludes with the NSTX-U Integrated System Test Procedure (ISTP-01) which establishes, tests, and documents the allowable NSTX-U operating parameters. ISTP-01 must be re-performed for any changes in those operating parameters.

The NSTX-U team is formulating the operational plan toward full operational capability for NSTX-U. In Table 10.3, a draft plan is shown based on assessment of physics needs for first year of operations. As shown in the table, the 1st year goal is to operate NSTX-U with the electromagnetic forces ($I_p B_T$) at halfway between NSTX and NSTX-U limits and 50% of the NSTX-U design-point of heating of any coil. This still allows NSTX to operate at $B_T \sim 0.8$ T, $I_p \sim 1.6$ MA, and the maximum flat-top duration of 3.5 s in the first year which is far beyond the achieved NSTX parameters. The device will be inspected and refurbished as needed at the end of the each operating year. For the second year, the toroidal magnetic field will be increased to its full field value of 1 T but keeping the heating of the coil to 75% of the design-point of any coil. This will allow 3 sec discharges at full field and current. The same limits should allow the full 5 sec discharges at $B_T \sim 0.8$ T, $I_p \sim 1.6$ MA. The device will be brought to full operational capability in the third year of NSTX-U operation. The proposed NSTX-U research operation weeks are shown in Fig. 10.2 and 10.3 depending on the budget scenarios. The operation weeks are reduced in FY 2016 and 2017 to accommodate the significant outage activities to install major upgrade hardware such as cryo-pump and divertor PFCs as shown in the figures.

	NSTX	Year 1 NSTX-U	Year 2 NSTX-U	Year 3 NSTX-U	Ultimate Goal
I_p [MA]	1.4	1.6	2.0	2.0	2.0
$I_p I_p$ [MA ²]	2.0	2.5	4.0	4.0	4.0
B_T [T]	0.55	0.8	1.0	1.0	1.0
$B_T B_T$ [T ²]	0.3	0.65	1.0	1.0	1.0
$I_p B_T$ [MA*T]	0.61	1.3	2	2.0	2
Allowed $I^2 t$ Fraction On Any Coil	1.0	0.5	0.75	1.0	1.0
I_p Flat-Top at max. allowed $I^2 t$, I_p , and B_T [s]	~0.7	~3.5	~3.	5	5

Table 10.3. A draft NSTX-U operational plan toward full operational capability.

References

- [1] J. E. Menard, S. Gerhardt, M. Bell, et al., *Nucl. Fusion* **52**, 083015 (2012).
- [2] NSTX Upgrade Project Team.
- [3] J. Hosea, et al., *Phys. Plasmas* **15**, 056104 (2008).
- [4] G. Taylor et al., US-Japan RF Heating Physics Workshop, Nara, Japan, December 14, 2012.
- [5] T. Kariya, et al, *J. Infrared, Millimetre and Terahertz Waves* **32**, 295-310 (2011).
- [6] S. A. Sabbagh, J. Bialek, R.E. Bell, et al., *Nucl. Fusion* **44** (2004) 560.
- [7] R. Raman, et al., *IEEJ Transactions on Fundamentals and Materials*, Vol. **132**, No. 7 pp 468-471 (2012)
- [8] J. Canik et al., APS-DPP, PP8.00030 (2012).
- [9] J-K Park et al., IAEA FEC, EX P4-33 (2012), Submitted to Nuclear Fusion.
- [10] D. K. Mansfield, A. L. Roquemore, H. Schneider, et al., *Fusion Eng. and Design* **85**, 890 (2010).
- [11] H. W. Kugel, et al., *Physics of Plasmas* **15**, 056118 (2008).
- [12] C.H. Skinner et al., *J. Nucl. Mater.* (2013),
<http://dx.doi.org/10.1016/j.jnucmat.2013.01.136>.
- [13] R. Raman et al., IAEA FEC, EX P2-10 (2012), Submitted to Nuclear Fusion.
- [14] R.J. Fonck, et al., APS DPP (2012) **GO6 10**, Providence, Rhode island.
- [15] A. Diallo, B. LeBlanc et al., *Rev. Sci. Instrum.* **83**, 10D532 (2012);
doi: 10.1063/1.4740267
- [16] R.E. Bell, R. Feder, *Rev. Sci. Instrum.* **81**, 10D724 (2010).
- [17] T. M. Biewer, R. E. Bell, et al., *Rev. Sci. Instrum.* **75**, 650 (2004).
- [18] K. Tritz, D. J. Clayton, D. Stutman, et al., *Rev. Sci. Instrum.* **83**, 10E109 (2012).
- [19] D. Stutman, M. Finkenthal, et al., *Rev. Sci. Instrum.* **70**, 572 (1999)
- [20] F. M. Levinton, H. Yuh, *Rev. Sci. Instrum.* **79**, 10F522 (2008).
- [21] E.L. Foley and F.M. Levinton, *Journal of Physics: Conference Series* **227**(2010) 012007.
- [22] R. Barchfeld, C.W. Domier, et al., APS-DPP PP8.38 (2012)
- [23] D. R. Smith, R. J. Fonck, G. R. McKee, and D. S. Thompson, *Rev. Sci. Instrum.* **83**, 10D502 (2012)
- [24] J. Zhang, et al., *Plasma Phys. Control. Fusion* **55** (2013) 045011.
- [25] S.J. Zweben et al, *Phys. Plasmas* **17**, 102502 (2010).
- [26] S. P. Gerhardt, et al., NSTX-U Diagnostic Brainstorm Meeting, July 2011.
- [27] M. Podesta and R.E. Bell, *Rev. Sci. Instrum.* **83** (2012) 033505.
- [28] F. Levinton, et al., NSTX-U Diagnostic Brainstorm Meeting, July 2011.
- [29] Ben LeBlanc et al., NSTX-U Diagnostic Brainstorm Meeting, July 2011.
- [30] J.-W. Juhn, K. C. Lee, *Rev. Sci. Instrum.* **81**, 10D540 (2010)

- [31] L F Delgado-Aparicio, D Stutman, K Tritz, et al., *Plasma Physics and Controlled Fusion*, 49(8):1245, 2007.
- [32] D Kumar, M Finkenthal, D Stutman, et al., *Plasma Physics and Controlled Fusion*, 54(6):065010, 2012.
- [33] M.A. Jaworksi et al, *Fusion Eng. Design* **87** 1711 (2012)
- [34] R.J. Maqueda et al, *Nucl. Fusion* **50**, 075002 (2010)
- [35] C.N. Taylor, et al., *Rev. Sci. Instrum.* **83**, 10D703 (2012).
- [36] V.A. Soukhanovskii, et al., *Rev. Sci. Instrum.* **81**, 10D723 (2010).
- [37] F. Scotti, et al., *Rev. Sci. Instrum.* **83**, 10E532 (2012).
- [38] A.G. McLean, *et al. Rev. Sci. Instrum.* **83** 053706 (2012).
- [39] C. H. Skinner, et al., *Rev. Sci. Instrum* **81**, 10E102 (2010).
- [40] V. Soukhanovskii, et al., NSTX-U Diagnostic Brainstorm Meeting, July 2011
- [41] M. Podestà et al., *Rev. Sci. Instrum.* **79** 10E521 (2008)
- [42] A. Bortolon et al., *Rev. Sci. Instrum.* **81** 10D728 (2010)
- [43] D. Liu et al., *Rev. Sci. Instrum.* **77** 10F113 (2006)
- [44] S. S. Medley, et al., *Rev. Sci. Instrum.* **75** 3625 (2004)
- [45] W. U. Boeglin et al., *Rev. Sci. Instrum.* **81** 10D301 (2010)
- [46] D. S. Darrow, *Rev. Sci. Instrum.* **79**, 023502 (2008)
- [47] S. Kubota et al, *Rev. Sci. Inst.* **81**, 10D917 (2010)